Published OnlineFirst December 20, 2019; DOI: 10.1158/0008-5472.CAN-19-2732

Sustained Coevolution in a Stochastic Model of Cancer–Immune Interaction

Jason T. George[1,2,3] and Herbert Levine[1,2,4]

ABSTRACT

The dynamic interactions between an evolving malignancy and the adaptive immune system generate diverse evolutionary trajectories that ultimately result in tumor clearance or immune escape. Here, we create a simple mathematical model coupling T-cell recognition with an evolving cancer population that may randomly produce evasive subclones, imparting transient protection against the effector T cells. T-cell turnover declines and evasion rates together explained differences in early incidence data across almost all cancer types. Fitting the model to TRACERx evolutionary data argued in favor of substantial and sustained immune pressure exerted upon a developing tumor, suggesting that clinically observed incidence is a small proportion of all cancer initiation events. This dynamical model promises to increase our quantitative understanding of many immune escape contexts, including cancer progression and intracellular pathogenic infections.

Significance: The early cancer–immune interaction sculpts intratumor heterogeneity through the selection of immune-evasive clones. This study provides a mathematical framework for investigating the coevolution between an immune-evasive cancer population and the adaptive immune system.

Introduction

T-cell immunotherapy has revolutionized modern cancer therapy, delivering durable remission outcomes with higher rates of overall survival for many cancer subtypes (1, 2). The tumor–immune interaction is quite complex, determined by the recruitment of a variety of immune system effectors, and varies as a function of disease duration, progression, and subtype (3, 4). A majority of observed and therapeutic antitumor immunity is accomplished by the cytotoxic $CD8^+$ T-cell repertoire, wherein immune cells recognize tumor-associated antigens (TAA) present on the surface of cancer cells (5). Adequate recognition leads to elimination of the target cells and expansion of the recognizing T-cell clone. Consistent with theoretical expectations (6, 7), effective immune repertoire detection of TAAs has been empirically validated during natural cancer progression as well as in the postimmunotherapeutic setting (8, 9).

One critical phenomenon that determines ultimate disease outcome is immunosurveillance, which relates to the degree to which tumor progression (typically in the absence of immunotherapy) is controlled by cancer–immune coevolution. To date, a majority of our understanding of this complex interaction has been experimentally driven (10–13) with immunoediting and TAA negative selection driving early-stage disease (14, 15). Recognition of TAAs relies on immune system discrimination between self and non-self epitopes, which is largely achieved through host-directed tolerance mechanisms. First, thymic negative selection functions by deleting immature T cells, which recognize common self-epitopes, thereby imparting central tolerance to the T-cell repertoire (16). This process is incomplete, however, and necessitates subsequent peripheral tolerance mechanisms (17, 18). Peripheral tolerance, in contrast, relies on T-cell inhibition at a systems-level and is achieved whenever a threat is perceived to be small based on a lower detection limit (19).

The "growth-threshold conjecture" is a key defining feature of systems-level immune detection wherein the total rate of change, not level, of a growing threat is the limiting determinant of immune system recognition (20, 21). Consequently, pathogens with small individual growth rates may slowly expand to large population sizes before risking immune system detection, consistent with the observed indolent course of intracellular viral illnesses (22) and escape of slow-growth tumors (23, 24). The corresponding evolutionary trajectories that arise as a result of immune detection based on threat dynamics are quite diverse and have implications for disease prognosis (15, 25). A mathematical framework that formalizes the underlying probabilistic dynamics governing the tumor–immune interaction promises to shed light on this complex process and could ultimately be implemented to better guide patient-specific immunotherapy.

The idea of modeling tumor progression and, in particular, treatment evasion is not new. Well-established stochastic models have revolutionized our understanding of acquired drug resistance in the setting of targeted therapy, in part, by highlighting the importance of random mutant acquisition and clonal selection on the population level (26, 27). Prior studies have also analyzed tumor escape using ordinary differential equations to model the tumor–immune interaction (28–30). A more recent analysis investigated systems-level cancer-immune dynamics in a deterministic setting without taking into account any evasion (23). Because the immune repertoire and evading cancer population are both evolving systems capable of random and repeated recognition and evasion, stochastic analysis is a useful framework for conceptualizing tumor recognition by the adaptive immune system. We previously considered an extreme version of this problem, namely an adaptive immune analogue susceptible to permanent defeat by a single but durable stochastic evasion event (24). Here we consider a more realistic scenario and use it to interpret data regarding age incidence curves as well as tumor clonal evolution.

[1]Center for Theoretical Biological Physics, Rice University, Houston, Texas. [2]Department of Bioengineering, Rice University, Houston, Texas [3]Medical Scientist Training Program, Baylor College of Medicine, Houston, Texas. [4]Department of Physics, Northeastern University, Boston, Massachusetts.

Note: Supplementary data for this article are available at Cancer Research Online (http://cancerres.aacrjournals.org/).

Corresponding Authors: Jason T. George, Rice University, 6100 Main Street, Houston, TX 77005. Phone: 713-348-8121; Fax: 713-348-8125; E-mail: jason.thomas.george@gmail.com; and Herbert Levine, Phone: 617-373-2903; E-mail: herbert.levine@rice.edu

Cancer Res 2020;80:811–9

doi: 10.1158/0008-5472.CAN-19-2732

Published OnlineFirst December 20, 2019; DOI: 10.1158/0008-5472.CAN-19-2732

Specifically, we introduce an analytically tractable mathematical framework for modeling the interaction between an adaptive T-cell repertoire capable of repeated recognition and a cancer population that may repeatedly evolve mechanisms of immune evasion. We solve for the cancer escape and elimination probabilities analytically and provide a statistical framework to study the mean-variance profiles of observed cancer coevolutionary trajectories. We apply our model to early cancer evolutionary data and predict "common initiation and rare progression," wherein a majority of cancer-initiating events are controlled by an intact immune system, of which, only a small subset randomly escapes and leads to observed disease.

Quick Guide to Equations and Assumptions

Our basic tumor–immune model consists of clones of cancer cells with pure birth at rate r until they are detected by the immune system. Recognition may occur once the tumor has reached a minimal detection size m_0 and we work assuming either all clones are detected at size m_0 with a one-time detection probability q (referred to as deterministic detection) or an ongoing chance of detection at sizes above m_0 (adaptive detection). Once detection occurs, cells are killed at rate $d > r$, giving rise to a finite lifetime for that clone. There is also a probability per birth event $\mu << 1$ that the clone will give rise to an evasive tumor subclone. We previously investigated a simpler model that assumed evasion events to be complete and durable against recognition by all current and future T cells (24). Effectively, evading clones were rare but catastrophic cells that were invisible to the immune system, modeling an extreme event such as MHC-I downregulation. In general, it is more reasonable to assume that most evasion events impart transient escape via cancer antigen downregulation, for example, from recognition by the current dominant effector T-cell clone, with future detection of less-frequent or *de novo* TAAs possible by other T-cell clones.

We study here the clonal evolution that results from repeated recognition and evasion events. Elimination of the parent clone follows from its recognition and eventual elimination by the immune system. However, the cancer population evolves if it successfully acquires an immune-evasive daughter clone prior to elimination. This process repeats for each subsequent population until either elimination or escape occurs, and we refer henceforth to the periodic growth followed by detection and elimination as a recognition cycle. To accomplish this, we assume that any evasive clonal population has a chance of being detected upon maturity to detection size. A typical trace of the population dynamics generated by our model is shown in **Fig. 1A–C** where clones are created by evasion and die by detection over repeated cycles. Note that when the tumor population reaches some higher threshold M the cancer becomes clinically observable and "escapes" immune surveillance; in this simulation this occurs at around $t = 50$. Here the color code reflects subclones created during a specific cycle of the process. In general, a given clone can give rise to multiple evasive lineages during its lifetime. For the deterministic detection scheme, it is straightforward to argue (24) that the number of such daughter clones may be approximated by a Poisson distribution with parameter

$$\lambda = \mu m_0 d/(d - r). \tag{A}$$

Thus, the total evader "intensity," that is, the parameter governing the total number of clones produced at period n, is simply $\gamma_{n,j} = j\lambda$, where j is the number of evasive clones at period n. A generalization of this formula for the adaptive assumption is presented in the Supplementary Data. The model can therefore be framed as generalization of the Galton–Watson branching process, well-established in modeling biological systems (31–33), by the addition of possible cancer escape. The process thus eventually culminates in either escape to size M or complete eradication of the tumor. We shall refer to the expected per-capita progeny as the branching parameter. In the deterministic case, this value is simply λ from Eq. A.

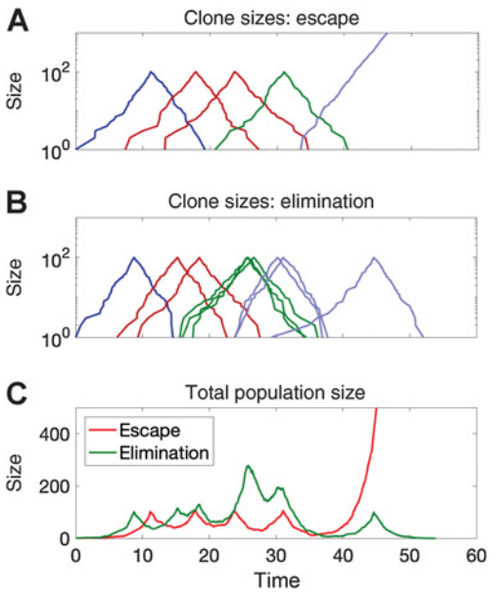

Figure 1.
Overview of coevolutionary trajectories. Simulations of the tumor–immune interactions depict clonal population sizes across recognition cycles (distinguished by different adjacent colors) in the event of ultimate escape (**A**) and elimination (**B**). The total population sizes are also recorded (**C**).

Instead of tracking the population size at a given time t along with the distribution of arriving clones (Supplementary Fig. S1), we focus instead on the number of evading clones, Z_n, per recognition cycle, n, starting from one initial clone (**Fig. 2A**). The clearance probability, or likelihood that a clone is recognized at cycle n, is denoted by q_n. This framework can in general handle any reasonable assumptions on the dependence of detection on cycle number. For example, it may be the case that the immune system becomes less capable over time due to exacerbation by an increasing number of unique clones. One could also generalize the above treatment to allow for the recognition rate to depend explicitly on the number of clones present at cycle n or even on the individual evasive clone as a function of its appearance order. These assumptions lead to an inhomogeneous Markov process relating the number of clones at cycle n to the number of clones at cycle $n + 1$ (**Fig. 2B** and **C**). For simplicity, we will mostly assume that q_n is a constant, which will be denoted as q_c, and in this case the Markov chain is homogeneous in cycle number. The probability of generating k clones in the next cycle given the existence of j clones in the current cycle is

$$p_{n+1,k} = p_k(\gamma_{n,j}) q_n^j, \tag{B}$$

with

$$p_k(\gamma_{n,j}) = e^{-\gamma_{n,j}} \gamma_{n,j}^k / k! \tag{C}$$

Published OnlineFirst December 20, 2019; DOI: 10.1158/0008-5472.CAN-19-2732

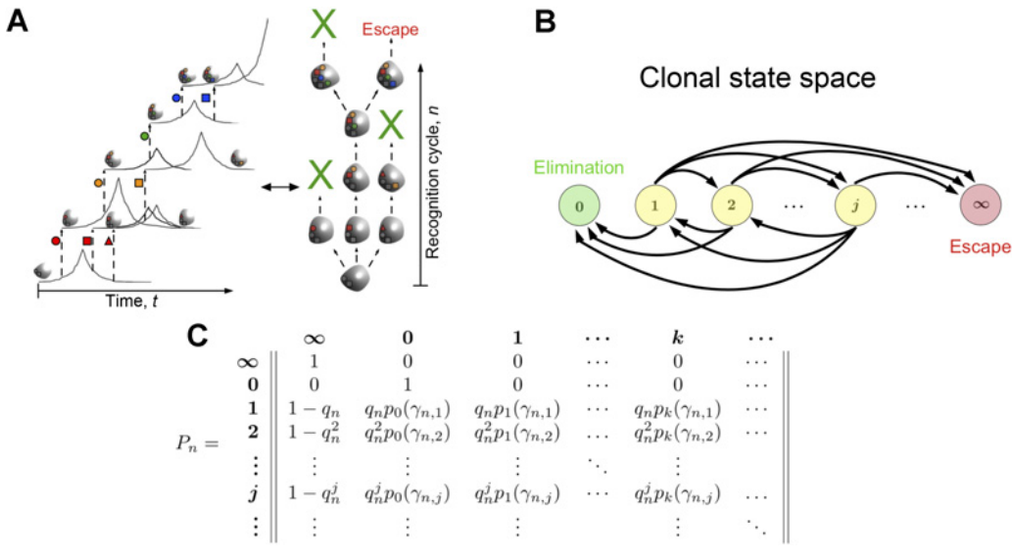

$$\begin{array}{c|cccccc} & \infty & 0 & 1 & \cdots & k & \cdots \\ \infty & 1 & 0 & 0 & \cdots & 0 & \cdots \\ 0 & 0 & 1 & 0 & \cdots & 0 & \cdots \\ 1 & 1-q_n & q_n p_0(\gamma_{n,1}) & q_n p_1(\gamma_{n,1}) & \cdots & q_n p_k(\gamma_{n,1}) & \cdots \\ 2 & 1-q_n^2 & q_n^2 p_0(\gamma_{n,2}) & q_n^2 p_1(\gamma_{n,2}) & \cdots & q_n^2 p_k(\gamma_{n,2}) & \cdots \\ \vdots & \vdots & \vdots & \vdots & \ddots & \vdots & \\ j & 1-q_n^j & q_n^j p_0(\gamma_{n,j}) & q_n^j p_1(\gamma_{n,j}) & \cdots & q_n^j p_k(\gamma_{n,j}) & \cdots \\ \vdots & \vdots & \vdots & \vdots & & \vdots & \ddots \end{array}$$

Figure 2.

Cancer–immune coevolutionary dynamics. **A,** A single initial clone grows, becomes recognized, and is eliminated, but not before producing immune evasive clones (distinguished by shapes), which impart transient immunity against the current effector T-cell clone. We assume that each evader has an independent opportunity to either escape or become recognized by the T-cell repertoire and may also give rise to additional evaders (evasion events occurring within the same recognition cycle share the same color and are differentiated by shape). **B,** The state space of this discrete process is the number of distinct evasive clones at each generational period. Escape (state ∞) and elimination (state 0) are absorbing states, and all other intermediate states communicate. **C,** This model may be represented in greatest generality by an inhomogeneous Markov process with a transition probability matrix that depends on the immune clearance probability, q_n^j, of each of the j clones at time n and the probability, $p_k(\gamma_{n,j})$, of generating k clones from j current clones, given by Eq. C.

The immune system must recognize every subclone at each period or else the threat escapes. Thus, for j clones at period n, the escape probability is

$$p_{n+1,\infty} = 1 - q_n^j. \quad \text{(D)}$$

Finally, the probability of tumor elimination is just the probability that no evasive clones are generated and no escape occurs, namely

$$p_{n+1,0} = q_n^j e^{-\gamma_{n,j}}. \quad \text{(E)}$$

Materials and Methods

All simulations, data analysis, and data visualization were performed using MATLAB version R2017b.

Escape and elimination probabilities

Derivations of the escape and elimination probabilities, together with the branching parameter, were solved using standard probabilistic analysis.

Simulations

All simulations of the evolutionary process were performed using a modified Gillespie algorithm. Analyses involving escape were simulated for all surviving populations until the emergence of a dominant clone that exceeded the upper clinical escape threshold.

Cancer age incidence

Age-specific cancer incidence data for breast, bladder, kidney, pancreas, prostate, head and neck, ovary, lung, melanoma, acute myeloid leukemia, and chronic lymphocytic leukemia were obtained from Cancer Research UK. Age incidence for triple-negative breast cancer was obtained by applying Web Plot Digitizer (34) to Fig. 1 of ref. 35 and taking a weighted average based on the empirical frequency of reported groups (Asian, $n = 368$; Black, $n = 509$; Hispanic, $n = 920$; White, $n = 2521$). Least-squares linear regression was performed on all available incidence data between ages 0 and 40 and in a similar manner between the age at which incidence is first measured and 40. The corresponding least-squares slope parameter is plotted for each cancer subtype against the mutation rate.

Evasion rates

Estimates of the per-cell mutation rates were obtained by using median rates from the available estimates from ref. 36 for acute myeloid leukemia (mutation rate $\mu = 3.33 \times 10^{-7}$; $n = 134$), bladder ($\mu = 5.17 \times 10^{-6}$; $n = 35$), breast cancer ($\mu = 9.33 \times 10^{-7}$; $n = 121$), chronic lymphocytic leukemia ($\mu = 7.67 \times 10^{-7}$; $n = 91$), head and neck cancer ($\mu = 3.17 \times 10^{-6}$; $n = 181$), lung cancer ($\mu = 7.20 \times 10^{-6}$; $n = 514$), melanoma ($\mu = 1.32 \times 10^{-5}$; $n = 121$), ovarian cancer ($\mu = 1.65 \times 10^{-6}$; $n = 394$), pancreatic cancer ($\mu = 1.07 \times 10^{-6}$; $n = 13$), prostate cancer ($\mu = 7.33 \times 10^{-7}$; $n = 227$), and renal cancer ($\mu = 1.53 \times 10^{-6}$; $n = 225$).

Statistical analysis

Correlations between the linear slope parameter of early cancer age incidence and per-cell evasion rates were assessed using Pearson correlation coefficient, and reported P values were obtained. For this, the null hypothesis was that there existed no correlation between the slope of early cancer age incidence and the per-cell evasion rate. Rejection of the null hypothesis and the presence of

Published OnlineFirst December 20, 2019; DOI: 10.1158/0008-5472.CAN-19-2732

significant (nonzero) correlation was assessed at a significance value of $\alpha = 0.05$.

TRACERx timing of evasion events

The time to most recent common ancestor relative to cancer initiating time for renal clear cell carcinoma was estimated from the TRACERx renal consortium using previously published data (37). The data were separated into two categories: evasion dominated by branching (samples K59, K167, K146, K065, K003, K150, K104, K163, K153, K126, K108, K135, K169, K139, K145, K156, K162, K180) and primarily linear evolution (samples K113, K165, K130, K023, K176, K037, K143, K124, K136, K096, K027, K158, K105) based on samples having their most recent common ancestor earlier or within 10 years of clinical detection, respectively. Mean and variance estimates of the mutational burden in patients with lung cancer were calculated from data reported in (38). Mean-variance frontiers were plotted assuming the quadratic relationship of Eq. J parameterized by some unknown fraction of relevant evasion events α, where we considered α up to 10%. Immune-enhanced, immune-compromised, and immune-neutral regions were defined by calculating all allowable mean-variance frontiers based on trajectories generated by the domain of interest.

Results

The following sections present the main findings of our analysis. Full mathematical details are provided in the Supplementary Data.

Escape and elimination probabilities

Let E_n (resp. F_n) be the event that the threat escapes (resp. is eliminated) at period n. One can directly derive a backwards discrete-time master equation that determines the long-time limit of these splitting probabilities. Specifically focusing on the elimination and taking $q = q_c$ to be constant, we have

$$P_k(F_n) = q_c^k \sum_{j=1}^{\infty} P_j(F_{n+1}) e^{-\lambda k} (\lambda k)^j / j!, \qquad \text{(F)}$$

where $P_k(F_n)$ is the probability that a tumor trajectory having k clones at cycle n eventually leads to complete tumor elimination. Clearly, each clone is independent from its future trajectory and hence $P_k(F_n) = P_1(F_n)^k$. Thus, Eq. F becomes a closed-form equation for $P_1(F_n)$

$$P_1(F_n) = q_c \sum_{j=1}^{\infty} P_1(F_{n+1})^j e^{-\lambda} \lambda^j / j! \qquad \text{(G)}$$

Taking the steady-state limit of this equation yields an equation for the asymptotic elimination probability p^*

$$p^* = q_c e^{-\lambda(1-p^*)} \qquad \text{(H)}$$

One can similarly find the asymptotic value of the escape probability and verify that it is just 1- p^*; in other words, the system always chooses one of the absorbing states in the long-time limit. A more complete treatment presented in the Supplementary Data allows this result to be extended to evaluate the full time-dependent value of $P_1(F_n)$ along with more general assumptions for the q_n.

The above outlines the model for the deterministic case since detection, should it occur, must do so at size m_0. Adaptive detection incorporates immune decline via an immunomodulatory parameter $\nu > 0$ that results in larger average detection sizes and yields a similar elimination probability $\tilde{p}^*$ (See Supplementary Data for full details). This analytic framework above agrees well with results obtained from simulating the full coevolutionary process (**Fig. 3A** and **B**). "Escape by underwhelming" is an important experimentally observed feature wherein threats of intermediate growth rates are at a survival disadvantage relative to their faster and slower growing counterparts (39). Our model recapitulates this behavior for minimal detection thresholds m_0 limited by the total cancer growth rate (**Fig. 3C**), in agreement with the growth-threshold conjecture (22). This simple theoretical framework generates a significant degree of diversity in dynamical behavior, governed completely by the clearance probability and the branching parameter (**Fig. 3D**; Supplementary Figs. S2–S10).

Our foundational model may also be adapted to investigate a variety of assumptions on the nature of immune escape, including declines in immune clearance as a function of elapsed time and total surviving clone numbers (Sec. S4.4, Intertemporal immune decline; Sec. S4.5, Clone frequency-dependent recognition) along with their effects on the likelihood of cancer elimination and escape (Supplementary Figs. S2 and S3). Prior empirical studies have proposed the existence of an equilibrium state, wherein a cancer population is neither fully eliminated nor grows to overwhelm the host (40, 41). Surprisingly, our framework would suggest that ultimate coexistence is not reasonably predicted, occurring only when unreasonable assumptions are imposed on the clearance probabilities (Sec. S4.3).

Differences in cancer early age incidence correlate with evasion rate

As proof-of-principle that local physiologic changes in immune function may affect observed cancer frequency, even among healthy individuals, we study the effects of physiologic declines in immune turnover on increases in early age incidence for various cancer types using publicly available large population datasets (Supplementary Fig. S6; ref. 42). Previous studies have shown that age-incidence data can be fit to simple models assuming a declining immune system with age (6, 43). Our dynamical model predicts, all else being equal, that tumor escape likelihoods vary directly as a function of evasion rate μ implicitly through the branching parameter. Although evasion need not be limited exclusively to genomic mechanisms, we use experimentally derived per-cell mutation rates obtained from a large pan-cancer analysis as an indirect measure of evasion (36).

We calculate the slope parameter of linear regression for early age incidence (**Fig. 4A**; Supplementary Fig. S6) and find a strong correlation between these values and the evasion rate. Aggregate breast cancer incidence appears to be an exception, perhaps a result of early screening detection and the incidence following puberty of hormone-sensitive disease. Restricting the comparison to triple negative breast cancer (35) reveals statistically significant correlation between incidence increases and evasion rate (**Fig. 4B**; Supplementary Fig. S7). Decreases in immune function modeled via an increased adaptive parameter ν (see Supplementary Data), assumed directly proportional to early age increases, result in increased ultimate escape probability, $1 - \tilde{p}^*$. We find excellent agreement in the predicted incidence slope-μ profile for the best-fit scaled range of immune function parameter ν (**Fig. 4C**). Moreover, using this normalized range for ν in the model predicts a linear increase in incidence for all observed mutation rates (**Fig. 4D**). Together, these findings demonstrate that cancer progression and escape are well-explained by variability in immune function across nearly all cancer types.

Evolutionary timing of renal clear cell carcinoma predicts prolonged coevolution with common tumor incidence and rare progression

Given the ability of our mathematical model to link observed cancer evasion and recognition cycle timing to underlying tumor–immune

Published OnlineFirst December 20, 2019; DOI: 10.1158/0008-5472.CAN-19-2732

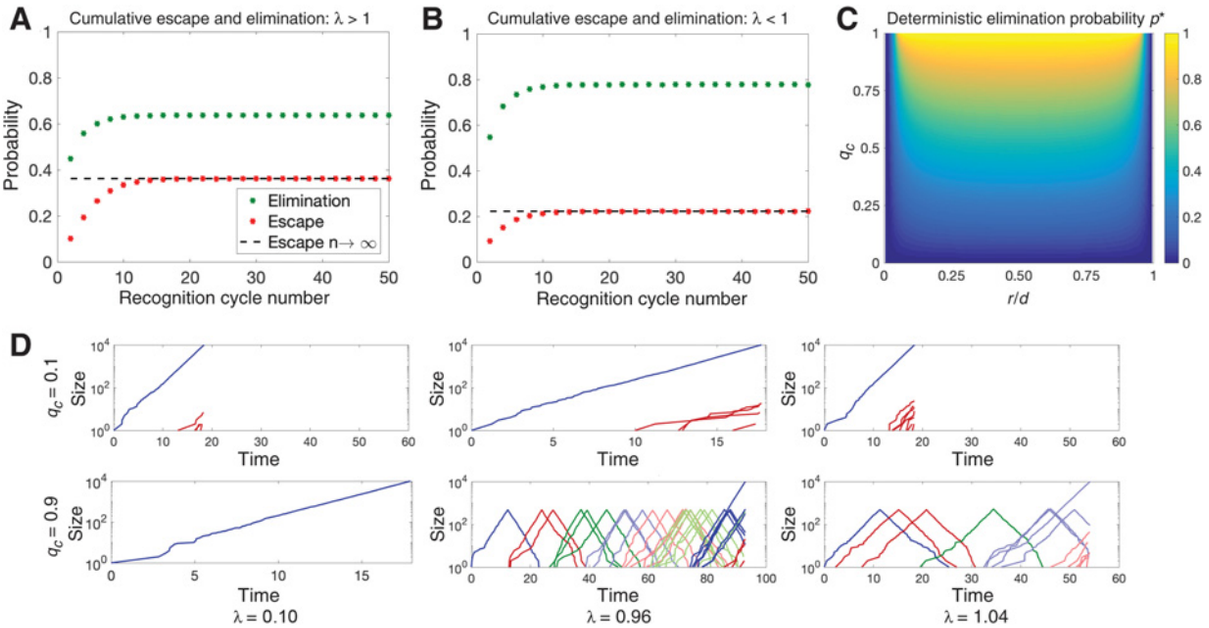

Figure 3.

General dynamics of the tumor–immune coevolutionary model. Escape (red) and elimination (green) probabilities are plotted as a function of recognition cycle number and compared to analytic escape (black dashed line), assuming supercritical ($\lambda = 1.04$; **A**) and subcritical ($\lambda = 0.96$; **B**) branching (in each case, $q_c = 0.95$ and simulations are averaged over 10^6 iterations). **C,** The dynamics induced by Eq. H permit a unique limiting elimination probability, p^*, which is plotted as a function of clearance probability and relative net growth rate (λ calculated using Eq. A, with $\mu = 10^{-6}$, $d = 0.2$, $R = 10^4$, and $m_0 = R/r$). **D,** A variety of evolutionary trajectories are plotted conditional on ultimate escape, assuming various clearance and branching parameters (in all cases, deterministic recognition was assumed, with $m_0 = 500$ and $r/d = 0.5$).

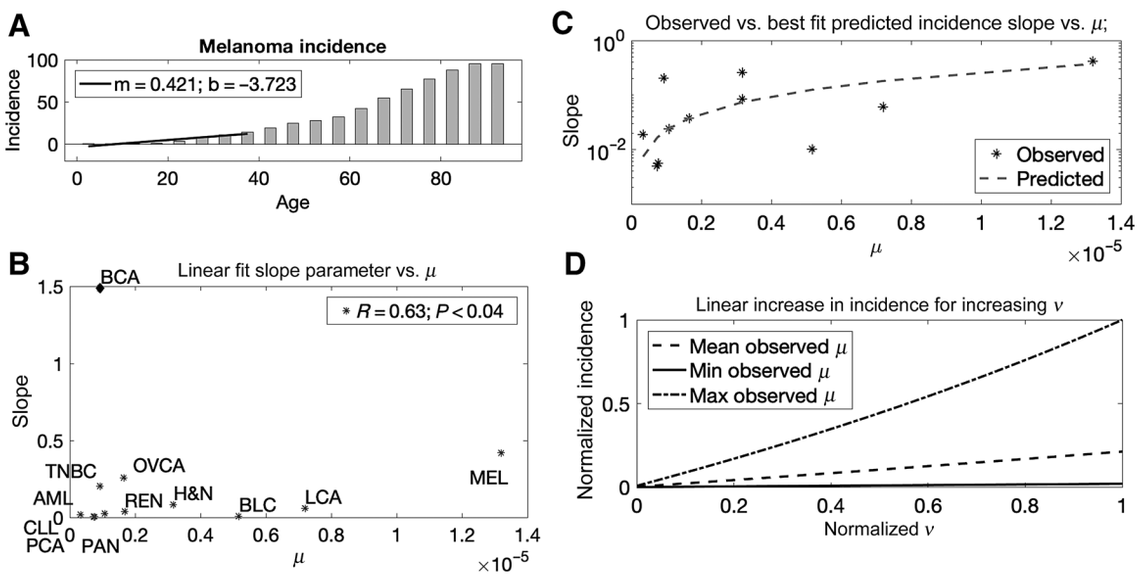

Figure 4.

Cancer incidence and evasion rate. **A,** The least-squares linear regression slope parameter of cancer early age incidence (between ages 0 and 40 years) is calculated for a variety of cancer subtypes (age at primary disease; melanoma shown); **B,** Rate of change in cancer early age incidence versus evasion rate. For each age incidence curve, linear regression is performed for incidence between ages 0 and 40 years. This parameter is plotted as a function of per-cell mutation rates for each cancer type. **C,** Assuming that the relationship between age and ν is linear, age = $k\nu$, the slope in cancer age-incidence can be calculated as a function of increasing ν, and are plotted for k that gives the least-squares error as compared with the experimental data. **D,** This parameterization consequently predicts linear increases in early cancer incidence as a function of diminished immune performance for all observed ranges of evasion rates μ.

Published OnlineFirst December 20, 2019; DOI: 10.1158/0008-5472.CAN-19-2732

coevolutionary dynamics, we next assessed the extent of immune evasion and clearance observed in cancer evolutionary data. The TRACERx renal clear cell carcinoma (RCCC) dataset (37) was particularly useful, providing estimates on the timing of landmark evolutionary events. Surprisingly, and consistent with model behavior under sustained control (**Fig. 3D**, $q_c = 0.9, \lambda = 0.96$), the authors found extended periods of clonal evolution sustained by small population sizes (estimated to be of order 10^2 cells). Using the arrival time of the most recent common ancestor (MRCA) as a representative of escape, we estimated the expected number of recognition cycles given the observed intervening time between MRCA detection and disease initiation. If t_m is the time it takes a clone to grow to minimal detection size $X(t_m) \sim 10^2$ and T_M is the times it takes to grow to ultimate detection size $X(t_m) \sim 10^9$, then the intervening time, assuming n recognition cycles occurs, is given by $\Delta t = t_M - nt_m$. From this, we can estimate the number of recognition cycles via

$$n = (7nt_m)/2(t_M - nt_m), \quad \text{(I)}$$

where nt_m and t_M are the observed times (see Supplementary Data for details). Our calculations predict that, on average, RCCC undergoes approximately 27 distinct, immunologically relevant recognition cycles prior to escape (**Fig. 5A** and **B**; Supplementary Fig. S11A).

The parameter range that generates this behavior is near criticality ($\lambda<1$) with high clearance probabilities (q_c approaching 1), suggesting effective immune handling of renal cell threats (**Fig. 5C**; Supplementary Fig. S11B). To further investigate the extent of immune protection, we used parameter estimates consistent with these findings to assess the frequency of observed cancer incidence relative to the total number of (unobserved) cancer-initiating events, and predict that initiation is 18 times as frequent as measured incidence. These results suggest that the adaptive immune system actively filters many potential threats manifesting as *de novo* initiating cancer clones, but may occasionally miss due to statistical chance, in support of the "bad-luck hypothesis" (44). The resulting population dynamics closely resemble those observed in the cancer incidence data, with a large disease period consisting of clonal evolution with low tumor burden, followed by either elimination or escape with extensive subclonal evolution (**Fig. 5D**). When separating samples into categories based on extensive linear or branched evolution and repeating this analysis, we find that patients with disease dominated by linear evolution are predicted to have significantly larger cycle numbers (57 ± 35) with a concomitant increase in the number of predicted initiating events relative to observed incidence. This behavior contrasts with trajectories dominated by branched evolution, which have a reduced cycle number (5 ± 2) with increased escape probability (Supplementary Fig. S12).

Fluctuations in lung cancer preceding escape partition disease subtypes based on immune function

Given the predicted implications of immune performance on eliminating early and indolent disease, we wanted to investigate the relationship between disease subtype and predicted immune status. Available data on large cohort patients with lung cancer (38) provided enough samples for each studied subtype to estimate mean and variance profiles for the distribution of clonal mutational events. This analysis was repeated for each lung cancer subtype and then compared with all predicted values

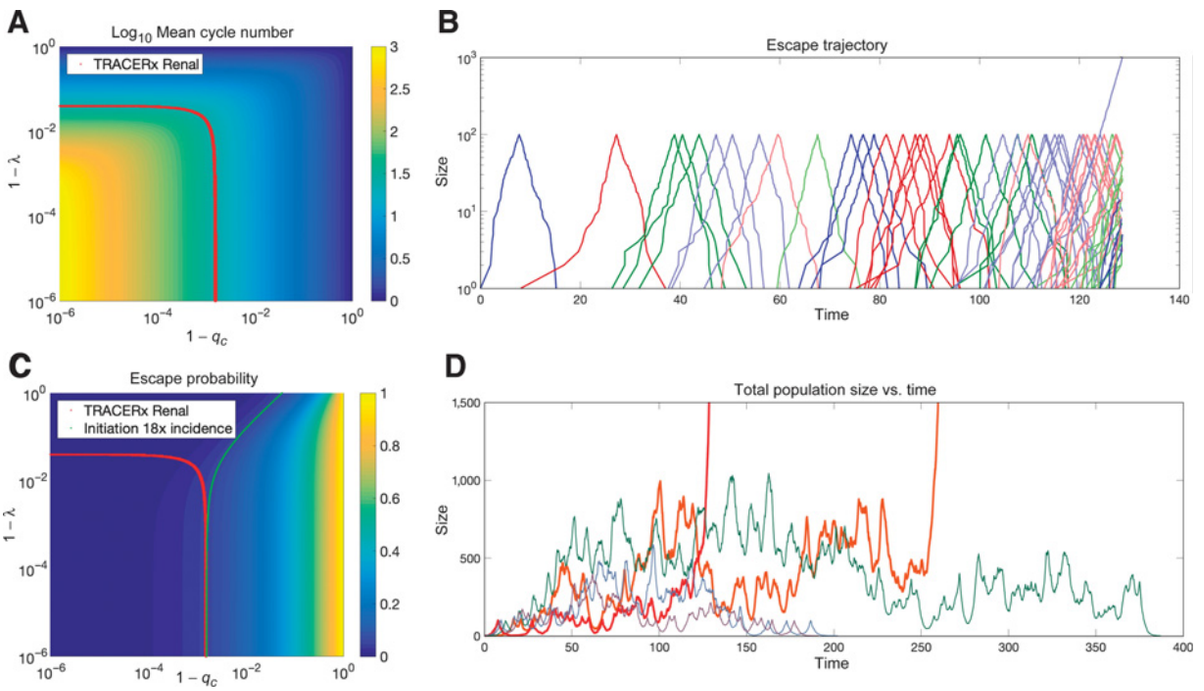

Figure 5.

Evolutionary dynamics of renal clear cell carcinoma. **A,** Relative timing of the TRACERx renal time to MRCA versus time to clinical escape implies an average of 26.6 recognition cycles, which restricts the range of allowable values of q_c and λ in the coevolution model (red line traces the contour line for relevant mean cycle number). **B,** A typical stochastic realization of the clonal branching that occurs in the deterministic case before and after escape (colors distinguish adjacent subclones arising within the same cycle number). **C,** Minimal values of observed clearance probability provide an upper estimate for the observed escape probability at 1/18 (plotted as a function of q_c and λ; green line traces the contour line for relevant escape probabilities). **D,** Simulation output of the total population size as a function of time for various realizations of the process.

Published OnlineFirst December 20, 2019; DOI: 10.1158/0008-5472.CAN-19-2732

in the model. Because only a small (unknown) fraction $\alpha << 1$ of total mutations are expected to impart immune evasion, we consider the resulting allowable mean-variance frontier assuming a range of small α. Very briefly, for X being the total number of clonal nonsynonymous mutational events with respective mean and variance given by μ_X and σ_X^2, the mean and variance for the fraction αX that are relevant to immune evasion relate to the observed parameters μ_X and σ_X^2 via

$$\begin{aligned}\mathbb{E}[\alpha X] &= \mu_X \alpha;\\ \mathbb{V}\mathrm{ar}(\alpha X) &= \sigma_X^2 \alpha^2.\end{aligned} \tag{J}$$

Equation J defines a quadratic mean–variance curve parameterized by α that can be applied to compare the observed curves against all allowable simulated parameters in the domain considered (**Fig. 5A** and **C**) to determine model conditions that are consistent with empirical data. Our above model defines a baseline relationship that well characterizes the reported mean-variance profiles across all lung cancer evolutionary data subtypes (**Fig. 6**; Supplementary Table S1). However, several variations in the mean-variance frontier are only achievable in our generalized model assuming either immune suppression or heightened immune surveillance (see Supplementary Data for full details). Interestingly, squamous cell carcinoma, and to a lesser extent positive smoking status, are more consistent with a process that is significantly immunosuppressed, suggesting that the observed pattern of mutational variability emerges in the setting of reduced immune targeting efficiency. Intriguingly, the predicted mean-variance frontier requires enhancements to immune clearance rates over successive periods to explain the nonsmoker signature (Eq. S123).

Discussion

The underlying early clonal architecture of an evolving cancer population contains a significant amount of information related to cancer progression and the extent of immunosurveillance. Understanding this complex behavior is essential for better predicting the extent of tumor immunoediting, measuring the frequency of disease progression relative to incidence, estimating immune targeting efficacy, and proposing optimized treatment strategies conditioned on post-escape clonal distributions. Here, we developed a stochastic population dynamical model of the battle between an evolving cancer population and the $CD8^+$ T-cell immune repertoire. Prior models of the cancer–immune interaction have explicitly represented and tracked immune effectors as a distinct population (22, 29). While useful for describing population control in a variety of contexts, including nonimmunogenetic tumors where immune evasion is a nondominant contributor to cancer progression, this approach falls short in characterizing the phylogenetic architecture and elimination probabilities of evasive cancer subclones following recognition via the adaptive immune system. Our alternative formulation explicitly models recognition on the population level assuming that the cancer compartment may randomly acquire evasive clones, each of which requires distinct T-cell clones in the immune repertoire for recognition and control. We made the implicit assumptions that cancer adaptivity is represented by an evasion rate μ, while immune system adaptivity depends on the repertoire diversity and turnover rates. The resulting tumor escape or elimination behavior is thus reduced to an effective branching parameter, λ. This framework is sufficiently general for studying the coevolution of tumor and immune system, in addition to formulating the key issue of immune escape and elimination with regards to the ability of the immune repertoire to keep pace with a heterogeneous and evading cancer population.

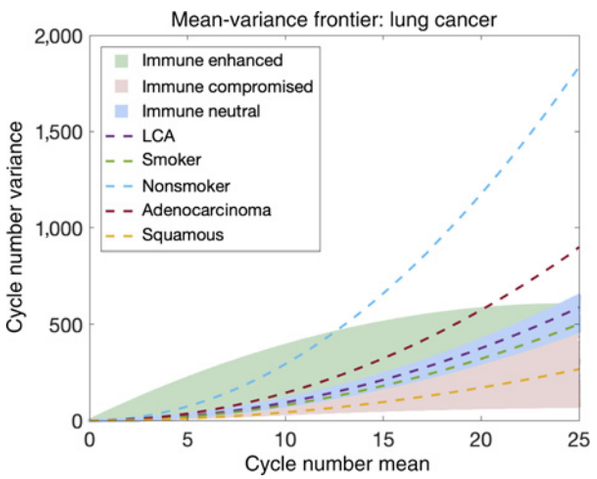

Figure 6.

Mean-variance frontiers for lung cancer subtypes. Empirical mean-variance frontiers are plotted using Eq. J and observed data for various LCA subtypes (dashed lines). These are compared with predicted allowable regions in the mean-variance space based on all parameter combinations studied in **Fig. 5A** and **C** (colored regions). Blue region corresponds with allowable frontiers, assuming deterministic recognition ($\nu = 0$). Red region highlights areas of nonoverlap in adaptive recognition where immune recognition is impaired ($\nu = 10$ taken to be 10% of m_0). Green regions represent dynamics assuming immune enhancement over time ($p_{c,n+1} = \max\{p_{c,\infty}, p_{c,n} + (p_{c,n} - p_{n,\infty}/25)\}$ for $p_{c,\infty} = 0.9$).

Previous empirical studies have proposed the existence of an equilibrium state wherein a growing cancer population can be maintained indefinitely (40, 41). In contrast, our model only predicts ultimate equilibrium for the unlikely case in which recognition rates of new clones increase dramatically as an increasing function of total clone number. More realistic assumptions on the decline in immune recognition, occurring either over time or when overwhelmed by a greater number of competing clones, prevents the cancer population from reaching ultimate equilibrium and implies that the immune recognition process ultimately results in either escape or elimination with certainty, given sufficient time.

The model's underlying dynamical behavior subsequently encodes information on both the likelihood and timing of ultimate cancer escape or elimination. Our framework highlights the importance of immunosurveillance in early disease progression as evidenced by differential increases in cancer incidence that scale with evasion rate across nearly all cancer types. We utilized per-cell mutation rates as an indirect measure of evasion capacity. Our findings were consistent despite changing the age range used as input for the linear regression. Indeed, many mutations are independent of immune evasion events and may increase the antigenic burden of the cancer population. This framework only distinguishes progeny based on an evasion event, which results in alteration or removal of an immune target recognized on the parent clone. Evaluating the competing effects of advantageous antigen down-regulation and undesirable tumor neoantigen generation on overall recognition by the immune system is an important consideration and warrants further investigation.

Using the excellent data available on the timing of early evolutionary events in RCCC, together with the observation that early clonal evolution is estimated to be sustained at small cell sizes, we show that the mean number of recognition cycles is quite large, suggestive of a drawn-out competition between immune and cancer compartments. Our results suggest that cancer progression from early initiation to

Published OnlineFirst December 20, 2019; DOI: 10.1158/0008-5472.CAN-19-2732

appreciable disease only occurs a small fraction of the time, in support of our proposed "common initiation and rare progression" postulate, wherein most cancer initiating events are effectively controlled by host recognition mechanisms. In the minority of cases where the cancer population escapes, our analysis predicts this to be due to random chance, consistent with the "bad-luck" hypothesis (44). Moreover, partitioning of samples into groups based on trajectories dominated by linear versus branched evolution revealed differences in mean recognition cycle and relative escape likelihood, the latter group characterized by punctuated evolution and early disease. We remark that these results are most sensitive to the assumed minimal population size (here taken to be $m_0 = 10^2$ as estimated empirically); the resulting mean cycle number estimate scales as a decreasing function of m_0 as $2/\log_{10} m_0$. Despite this, significant and prolonged coevolution is still predicted (15 recognition cycles in renal cancer patients) assuming an order of magnitude increase in the minimal detection size. Although empirically challenging, further investigation into the early tumor–immune interaction following initiation could refine this estimate and shed light on the underlying evolution of early disease for a variety of cancers. When comparing the mean-variance frontiers in the clonal distributions of TRACERx LCA subtypes, we found that observed evolutionary trajectories for squamous cell carcinoma and positive smoking status were consistent with simulated profiles assuming immune impairment, while nonsmokers and adenocarcinoma followed an opposite trend. Our results demonstrate the utility of further experimental investigation into the benefit of distinct treatment strategies based on cancer subtype and predicted immune function of each patient.

Cancer evolution is complex and highly variable owing to the dynamic interaction that occurs between tumor cells and the adaptive immune system. Improvement in our understanding of cancer progression therefore requires a detailed description of individual disease evolutionary trajectories. Toward this end, we have developed a mathematical framework that models a heterogeneous population of cancer cells subjected to adaptive immunosurveillance. When applied to empirical data, our model is a useful tool for studying the tumor–immune interaction as it establishes a fundamental relationship between evasion and the observed branching structure that emerges during disease progression. Although we have focused our analysis on describing the control and progression of cancer, our model is broadly applicable in understanding similar phenomena, such as intracellular infection by pathogens that evolve mechanisms of immune evasion. In HIV, for example, the delayed minimal disease burden produced by repeated recognition cycles in our model shares some general features of the latent period (45). Future efforts to apply this model in a broader context may provide insights regarding the observed dynamics of slow-progression intracellular threats.

Disclosure of Potential Conflicts of Interest

No potential conflicts of interest were disclosed.

Authors' Contributions

Conception and design: J.T. George, H. Levine
Development of methodology: J.T. George, H. Levine
Acquisition of data (provided animals, acquired and managed patients, provided facilities, etc.): J.T. George
Analysis and interpretation of data (e.g., statistical analysis, biostatistics, computational analysis): J.T. George, H. Levine
Writing, review, and/or revision of the manuscript: J.T. George, H. Levine
Study supervision: J.T. George

Acknowledgments

We would like to thank Jeffrey Molldrem for fruitful discussions on immunotherapy and cancer-immune coevolution.

J.T. George is supported by the NCI of the NIH (F30CA213878). H. Levine is supported by Physics Frontiers Center NSF Grant PHY-1427654 and by NSF PHY-1605817.

The costs of publication of this article were defrayed in part by the payment of page charges. This article must therefore be hereby marked *advertisement* in accordance with 18 U.S.C. Section 1734 solely to indicate this fact.

Received August 31, 2019; revised November 15, 2019; accepted December 18, 2019; published first December 20, 2019.

References

1. Couzin-Frankel J. Cancer immunotherapy. Science 2013;342:1432–3.
2. Luke JJ, Flaherty KT, Ribas A, Long GV. Targeted agents and immunotherapies: optimizing outcomes in melanoma. Nat Rev Clin Oncol 2017;14:463.
3. De Visser KE, Eichten A, Coussens LM. Paradoxical roles of the immune system during cancer development. Nat Rev Cancer 2006;6:24.
4. Finn O. Immuno-oncology: understanding the function and dysfunction of the immune system in cancer. Ann Oncol 2012;23:viii6–9.
5. Coulie PG, Van den Eynde BJ, Van Der Bruggen P, Boon T. Tumour antigens recognized by t lymphocytes: at the core of cancer immunotherapy. Nat Rev Cancer 2014;14;135.
6. George JT, Kessler DA, Levine H. Effects of thymic selection on t cell recognition of foreign and tumor antigenic peptides. Proc Natl Acad Sci U S A 2017;114:E7875–81.
7. Mayer A, Balasubramanian V, Walczak AM, Mora T. How a well-adapting immune system remembers. Proc Natl Acad Sci U S A 2019;116:8815–23.
8. Yadav M, Jhunjhunwala S, Phung QT, Lupardus P, Tanguay J, Bumbaca S, et al. Predicting immunogenic tumour mutations by combining mass spectrometry and exome sequencing. Nature 2014;515:572.
9. Zamora AE, Crawford JC, Thomas PG. Hitting the target: how t cells detect and eliminate tumors. J Immunol 2018;200:392–9.
10. Ott PA, Hu Z, Keskin DB, Shukla SA, Sun J, Bozym DJ, et al. An immunogenic personal neoantigen vaccine for patients with melanoma. Nature 2017;547:217–21.
11. Sahin U, Derhovanessian E, Miller M, Kloke BP, Simon P, Löwer M, et al. Personalized rna mutanome vaccines mobilize poly-specific therapeutic immunity against cancer. Nature 2017;547:222–6.
12. Leach DR, Krummel MF, Allison JP. Enhancement of antitumor immunity by ctla-4 blockade. Science 1996;271:1734–6.
13. Sadelain M, Rivière I, Riddell S. Therapeutic T cell engineering. Nature 2017;545:423–31.
14. Fridman WH, Mlecnik B, Bindea G, Pagès F, Galon J. Immunosurveillance in human non-viral cancers. Curr Opin Immunol 2011;23:272–8.
15. Rosenthal R, Cadieux EL, Salgado R, Al Bakir M, Moore DA, Hiley CT, et al. Neoantigen-directed immune escape in lung cancer evolution. Nature 2019;567:479–85.
16. Nossal G. Negative selection of lymphocytes. Cell 1994;76:229–39.
17. Davis MM. Not-so-negative selection. Immunity 2015;43:833–5.
18. Legoux FP, Lim JB, Cauley AW, Dikiy S, Ertelt J, Mariani TJ, et al. Cd4+ t cell tolerance to tissue-restricted self antigens is mediated by antigen-specific regulatory t cells rather than deletion. Immunity 2015;43:896–908.
19. Grossman Z, Paul WE. Adaptive cellular interactions in the immune system: the tunable activation threshold and the significance of subthreshold responses. Proc Natl Acad Sci U S A 1992;89:10365–9.
20. Pradeu T, Jaeger S, Vivier E. The speed of change: towards a discontinuity theory of immunity? Nat Rev Immunol 2013;13:764–9.
21. Johansen P, Storni T, Rettig L, Qiu Z, Der-Sarkissian A, Smith KA, et al. Antigen kinetics determines immune reactivity. Proc Natl Acad Sci U S A 2008;105:5189–94.
22. Arias CF, Herrero MA, Cuesta JA, Acosta FJ, Fernandez-Arias C. The growth threshold conjecture: a theoretical framework for understanding T-cell tolerance. R Soc Open Sci 2015;2:50016.

23. Sontag ED. A dynamic model of immune responses to antigen presentation predicts different regions of tumor or pathogen elimination. Cell Syst 2017;4: 231–41.
24. George JT, Levine H. Stochastic modeling of tumor progression and immune evasion. J Theor Biol 2018;458:148–55.
25. Dunn GP, Bruce AT, Ikeda H, Old LJ, Schreiber RD. Cancer immunoediting: from immunosurveillance to tumor escape. Nat Immunol 2002;3:991.
26. Iwasa Y, Nowak MA, Michor F. Evolution of resistance during clonal expansion. Genetics 2006;172:2557–66.
27. Michor F, Iwasa Y, Nowak MA. Dynamics of cancer progression. Nat Rev Cancer 2004;4:197–205.
28. Al-Tameemi M, Chaplain M, dOnofrio A. Evasion of tumours from the control of the immune system: consequences of brief encounters. Biol Direct 2012;7:31.
29. de Pillis LG, Radunskaya AE, Wiseman CL. A validated mathematical model of cell-mediated immune response to tumor growth. Cancer Res 2005;65:7950–8.
30. Grossman Z, Berke G. Tumor escape from immune elimination. J Theor Biol 1980;83:267–96.
31. Athreya KB, Ney PE. Branching Processes. New York: Springer Science & Business Media, 2012.
32. Karlin S. A first course in stochastic processes. San Diego: Academic Press, 2014.
33. Grimmett G, Grimmett GR, Stirzaker D, et al. Probability and random processes. New York: Oxford University Press, 2001.
34. Rohatgi A. Webplotdigitizer. 2011. https://automeris.io/WebPlotDigitizer/.
35. Kurian AW, Fish K, Shema SJ, Clarke CA. Lifetime risks of specific breast cancer subtypes among women in four racial/ethnic groups. Breast Cancer Res 2010;12: R99.
36. Lawrence MS, Stojanov P, Polak P, Kryukov GV, Cibulskis K, Sivachenko A, et al. Mutational heterogeneity in cancer and the search for new cancer-associated genes. Nature 2013;499:214.
37. Mitchell TJ, Turajlic S, Rowan A, Nicol D, Farmery JH, OBrien T, et al. Timing the landmark events in the evolution of clear cell renal cell cancer: TRACERx renal. Cell 2018;173:611–23.
38. Jamal-Hanjani M, Wilson GA, McGranahan N, Birkbak NJ, Watkins TB, Veeriah S, et al. Tracking the evolution of non–small-cell lung cancer. N Engl J Med 2017;376:2109–21.
39. Bocharov G, Ludewig B, Bertoletti A, Klenerman P, Junt T, Krebs P, et al. Underwhelming the immune response: effect of slow virus growth on CD8+ T-lymphocyte responses. J Virol 2004;78:2247–54.
40. Dunn GP, Old LJ, Schreiber RD. The three es of cancer immunoediting. Annu Rev Immunol 2004;22:329–60.
41. Teng MW, Swann JB, Koebel CM, Schreiber RD, Smyth MJ. Immune-mediated dormancy: an equilibrium with cancer. J Leukoc Biol 2008;84: 988–93.
42. Acute myeloid leukaemia (aml) incidence by age (2013). Available from: http://www.cancerresearchuk.org/health-professional/cancer-statistics.
43. Palmer S, Albergante L, Blackburn CC, Newman T. Thymic involution and rising disease incidence with age. Proc Natl Acad Sci U S A 2018;115: 1883–8.
44. Tomasetti C, Vogelstein B. Variation in cancer risk among tissues can be explained by the number of stem cell divisions. Science 2015;347:78–81.
45. Siliciano RF, Greene WC. HIV latency. Cold Spring Harb Perspect Med 2011;1: a007096.

Cancer Research
The Journal of Cancer Research (1916–1930) | The American Journal of Cancer (1931–1940)

AACR American Association for Cancer Research

Sustained Coevolution in a Stochastic Model of Cancer–Immune Interaction

Jason T. George and Herbert Levine

Cancer Res 2020;80:811-819. Published OnlineFirst December 20, 2019.

Supplementary Information: Sustained Co-Evolution in a Stochastic Model of the Cancer-Immune Interaction

Jason T. George and Herbert Levine

November 12, 2019

S1 Overview

Here we lay the general theoretical groundwork for studying stochastic co-evolution between the adaptive immune system and a threat like cancer that may acquire immune evasive phenotypes. We build on our earlier model that studied immune recognition in the special case that a threat acquires complete immune evasion, such as via MHC-I down-regulation. This time, we study intermediate levels of evasion and account for the possibility of continual, adaptive recognition. Sec. S2 provides a brief outline of the model. Sec. S3 states the transition probability matrix for the most general model. Sec. S2.3 solves for escape and elimination probabilities for this model when detection size is assumed fixed, while Sec. S5 considers the case when detection size may vary stochastically for each clone. Sec. S6 discusses observed evolution following escape, and Sec. S7 concludes by providing an application of the model to cancer age incidence data and characterizes early evolutionary trajectories of renal clear cell carcinoma and non-small cell lung cancer.

S2 Model development

Previously, we proposed and investigated a mathematical model of cancer-immune interaction under adaptive immunosurveillance limited by the a lower threshold determined by the tumor net growth rate. We demonstrated consistency between this framework and empirical observations, including 'sneak-through' of slow-growth threats, AML age-specific incidence, and increases in incidence corresponding to poorer immune function [1]. This framework considered tumor evasion and immune escape for two phenotypes: immune-detectable cells with intact mechanisms of antigen presentation, and rare but devastating immune-evasive cells that had evolved mechanisms for complete adaptive immune evasion. Here, we wish to extend the analysis to a (possibly large) collection of clonally diverse tumor populations, each with an intermediate evasion potential. We distinguish each clone based on sufficient phenotypic diversity from any prior progenitors so that the immune system must independently recognize it.

S2.1 Cancer population dynamics

Previously, we investigated systems having 'all-or-none' immune evasion potential. Evasion, if it occurred, automatically resulted in population escape. The relevant parameters for this two-compartment model included a sensitive (type-1) cell population, $y_1(t)$, and an evasive (type-2) population $y_2(t)$. Both cell types were assumed to divide at a per-cell rate of r, and type-1 cells had an evasion rate of $\mu \ll 1$. If type-1 cells were recognized by the immune system, then they were eliminated at a per-cell rate of $\tilde{r} > 0$. Type-2 cells were incapable of subsequent recognition. If S_1 denotes the time of type-1 cell recognition, then transitions associated with this system can be written as:

$$\begin{aligned}
&t < S_1: \\
&\quad \big(y_1(t), y_2(t)\big) \to \big(y_1(t), y_2(t)+1\big) \text{ at rate } \mu r y_1(t) + r y_2(t) \\
&\quad \big(y_1(t), y_2(t)\big) \to \big(y_1(t)+1, y_2(t)\big) \text{ at rate } (1-\mu) r y_1(t) \approx r y_1(t) \\
&t \geq S_1: \\
&\quad \big(y_1(t), y_2(t)\big) \to \big(y_1(t), y_2(t)+1\big) \text{ at rate } \mu r y_1(t) + r y_2(t) \\
&\quad \big(y_1(t), y_2(t)\big) \to \big(y_1(t)-1, y_2(t)\big) \text{ at rate } [d-(1-\mu)r] y_1(t) \approx \tilde{r} y_1(t)
\end{aligned} \tag{S1}$$

Here, our primary goal focuses on a generalized framework for studying systems evolving intermediate evasion states that may confer temporary immune shielding, but may also be recognized following additional turnover in the adaptive immune compartment. As above, each clonal population undergoes net birth that is either unopposed, resulting in escape, or is followed by recognition and subsequent immune killing. Each cell has an evasion rate of $\mu \ll 1$ per division per cell. At a given time, with $W(t)$ total clones observed over the growth history, let $y_i(t)$ be the population of the i^{th} clone, and S_i the (random) time of recognition. Then the i^{th} clone evolves according to the dynamics

$$\begin{aligned}
&t < S_i: \big(y_1(t), \dots, y_i(t), \dots, y_{W(t)}(t), 0, \dots\big) \to \big(y_1(t), \dots, y_i(t)+1, \dots, y_{W(t)}(t), 0, \dots\big), \\
&\qquad \text{at rate } (1-\mu) r y_i(t) \approx r y_i(t); \\
&t \geq S_i: \big(y_1(t), \dots, y_i(t), \dots, y_{W(t)}(t), 0, \dots\big) \to \big(y_1(t), \dots, y_i(t)-1, \dots, y_{W(t)}(t), 0, \dots\big), \\
&\qquad \text{at rate } [d-(1-\mu)r] y_i(t) \approx \tilde{r} y_i(t),
\end{aligned} \tag{S2}$$

with new clones arriving according to

$$(y_1(t), \dots, y_W(t), 0, \dots) \to (y_1(t), \dots, y_{W(t)}(t), 1, 0, \dots) \text{ at rate } \mu r \sum_{i=1}^{W(t)} y_i(t). \tag{S3}$$

S2.2 Clonotype population dynamics

The above transitions are complicated to analyze analytically in part owing to the difficulty in tracking the origin of a possibly unbounded number of new clones. Instead, we focus on the number of total clones Z_n present at a given recognition cycle. In contrast to $W(t)$, which is nondecreasing in time and counts clones of zero size, Z_n records the current number of non-extinct clones. We define the n^{th} recognition cycle to be n-time steps following the growth and elimination of the founder clone. In this way, every evasive clone arising from the founder population is assigned to recognition cycle $n = 1$ (red clones in Fig. 2A). The founder population $y_1(t)$ either escapes, or is recognized and eliminated by time $\tilde{S}_1$ and discrete period $n = 1$, possibly generating X_1 distinct evasive clones. The number of clones initially is $Z_0 = 1$ and the number after the first recognition cycle is $Z_1 = X_1$. Each new evading clone has an independent chance of escaping. If this occurs, the process ends, but otherwise all clones are recognized and become extinct by period $n = 2$. This process continues, and the number of clones present at the n^{th} discrete time step is Z_n.

In shifting our focus from the continuous-time population size dynamics to the embedded, discrete-time clonal structure, we are able to characterize clonal evolution and escape as a branching process for each recognition cycle [2, 4]. We assume no bound on the total population size for analytic convenience (the resulting effects of finite size restrictions are considered in Sec. S6), and the process stops if either extinction or escape occurs. The state space, S, for Z_n is the non-negative integers and infinity,

$$S = \mathbb{Z}^+ \cup \{\infty\}, \tag{S4}$$

where state $Z_n = 0$ corresponds to extinction of the cancer population, and $Z_n = \infty$ is the state of immune escape, meaning that at least one of the clones completely avoided the immune system. The latter representation of the escape state coincides with the notion that any given sub-clone can generate an unbounded number of progeny if it escapes and will be convenient for Secs. S4.1, S6. For clarity, we order our state space in the all analyses to follow according to $S = \{\infty, 0, 1, 2, \dots\}$.

S2.3 Deterministic recognition arrival rates

Under deterministic recognition with possible escape, the i^{th} clonal population at time n is either detected at some fixed size $y_i = m_0$ with probability $q_{n,i}$ or escapes detection altogether with probability $1 - q_{n,i}$. This generalizes our earlier framework where $n = 1$ always and we had assumed that $q_{1,1} = 1$ [1]. Prior modeling results imply that the number of new clones generated from a single clone during net growth to size m_0 prior to recognition ($t < S_i$) is well-characterized by a Poisson-distributed random variable with intensity μm_0, while post-recognition ($t \geq S_i$) clones arrive at an approximate intensity of $\mu m_0 r/(d-r)$ [1]. Thus the total number of new clones obtained from the i^{th} clone at period n is modeled as a Poisson-distributed random variable with parameter

$$\lambda = \mu m_0 d/(d-r) \equiv \lambda_0 m_0, \tag{S5}$$

so that $\lambda_0 \equiv \mu d/(d-r)$ describes the mean clone arrival rate for a population detected at size m_0. If there are j distinct clones present at period n, then the number of new clones in the next period is Poisson-distributed with parameter

$$\gamma_{n,j} = j\lambda \tag{S6}$$

as it is the sum of j IID Poisson replicates. Thus, the intensity of new clone arrivals is the product of clone number, population size at detection, and the per-population arrival rate.

S2.4 Stochastic recognition arrival rates

As in the deterministic case, the i^{th} clonal population at period n may be detected with probability $q_{n,i}$ or may escape with probability $1 - q_{n,i}$. Here however, recognition sizes are stochastic and allowed to occur at *any* clone population sizes larger than detection threshold m_0. In this case the intensity parameter characterizing the arrival of new clones is no longer fixed at λ as above, but instead a random variable itself, which we denote as $\Lambda_{n,i}$. This random parameter represents the average number of new clones obtained from the i^{th} clone at period n and may take values:

$$\Lambda_{n,i} \in \{\lambda_0 m_0, \lambda_0(m_0+1), \lambda_0(m_0+2), \dots\}. \tag{S7}$$

If there are j distinct clones present at period n, then the number of new clones at time $n+1$ is Poisson-distributed with random parameter $\Gamma_{n,j}$, given by

$$\Gamma_{n,j} = \sum_{i=1}^{j} \Lambda_{n,i}. \tag{S8}$$

In this framework, deterministic recognition is a special case of adaptive recognition where $\Gamma_{n,j} = j\lambda$ with probability one for each period n and total clone number j. Implicit in this setup is the assumption of unbounded clone sizes, albiet with rapidly decaying tail probabilities. This is a slight modification of our prior work, where we modeled escape probabilities related exclusively to the current repertoire [1]. Here, $q_{n,i}$ relates to lifetime immune escape at or beyond detection size $m \geq m_0$, and subsequently parameterizes the current and future immune repertoire. The underlying distribution governing $\Lambda_{n,i}$ relates strictly to variability (or impairment) in the ability of the repertoire to recognize threats close to the detection limit.

S2.5 Timing

As mentioned above, discrete periods in this framework are related (but not identical) to the elapsed time. We briefly outline the estimate of the arrival time of each clone in a given period. From previously [1], we have that the intensity of Poisson arrivals is given by

$$\eta(t) = \mu r i \tag{S9}$$

when there are i cells in a given clonal population. The inter-arrival times for the population at size i to grow (resp. shrink) by one, written ΔS_i (resp. $\Delta \tilde{S}_i$), may be approximated by their mean values $s_i = 1/ri$ (resp. $\tilde{s}_i = 1/\tilde{r}i$, with $\tilde{r} = d - r$). The probability density for the arrival time of the nth clone is given by

$$f_n(t) = \frac{m_\eta(t)^{n-1}(t)}{(n-1)!}\eta(t)e^{-m_\eta(t)}, \tag{S10}$$

where

$$m_\eta(t) \equiv \int_0^t \eta(\tau)d\tau, \tag{S11}$$

is the mean value function. This allows for a more detailed description of arrival times in the order of clone appearance. Distributions for the first five clones are plotted in Fig. S1.

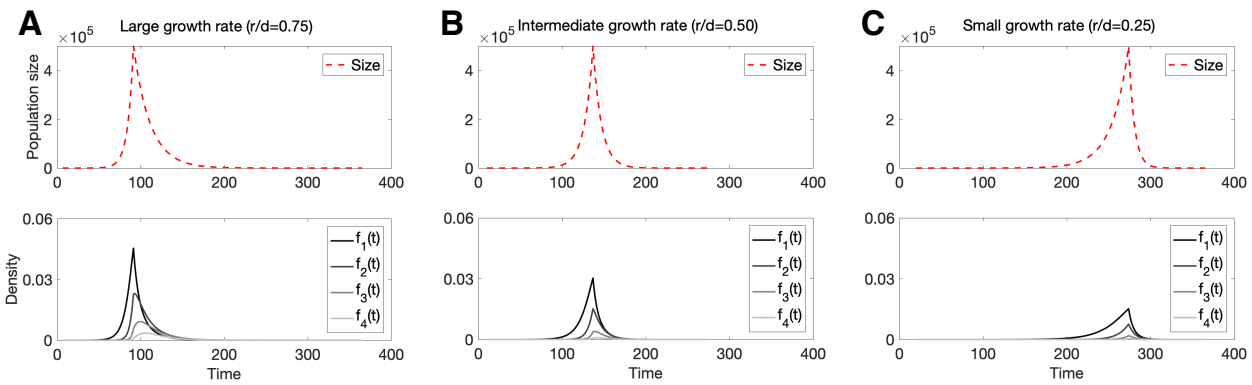

Figure S1: Distribution of inter-temporal clone arrival times. Population dynamics (red dashed lines) are compared to the distribution $f_n(t)$ of arrival times for the n^{th} clone (gray solid lines for the first five arrivals) with (A) $r = 0.05$, (B) $r = 0.10$, and (C) $r = 0.15$ ($d = 0.10$, $m_0 = 5 \cdot 10^5$, $\mu = 10^{-6}$.)

S3 General Framework

Let $\pi_{n,k}$ represent the probability of having k evasive clones after n recognition cycles. The discrete time Markov process is in general not time homogeneous, its evolution characterized by $\pi_{n+1} = \pi_n P_n$, with transition probability matrix $P_n = \mathbb{P}\big(Z_{n+1} = j \mid Z_n = k\big)$, given by:

$$P_n = \begin{array}{c|c|ccccc|c} & \boldsymbol{\infty} & \mathbf{0} & \mathbf{1} & \mathbf{2} & \cdots & \boldsymbol{k} & \cdots \\ \hline \boldsymbol{\infty} & 1 & 0 & 0 & 0 & \cdots & 0 & \cdots \\ \mathbf{0} & 0 & 1 & 0 & 0 & \cdots & 0 & \cdots \\ \mathbf{1} & 1-q_n & q_n p_0(\Gamma_{n,1}) & q_n p_1(\Gamma_{n,1}) & q_n p_2(\Gamma_{n,1}) & \cdots & q_n p_k(\Gamma_{n,1}) & \cdots \\ \mathbf{2} & 1-q_n^2 & q_n^2 p_0(\Gamma_{n,2}) & q_n^2 p_1(\Gamma_{n,2}) & q_n^2 p_2(\Gamma_{n,2}) & \cdots & q_n^2 p_k(\Gamma_{n,2}) & \cdots \\ \vdots & \vdots & \vdots & \vdots & \vdots & \ddots & \vdots & \\ \boldsymbol{j} & 1-q_n^j & q_n^j p_0(\Gamma_{n,j}) & q_n^j p_1(\Gamma_{n,j}) & q_n^j p_2(\Gamma_{n,j}) & \cdots & q_n^j p_k(\Gamma_{n,j}) & \cdots \\ \vdots & \vdots & \vdots & \vdots & \vdots & & \vdots & \ddots \end{array} \tag{S12}$$

where the q_n represent fixed probabilities for immune clearance of each clone at time n, and

$$p_k(\Gamma_{n,j}) = e^{-\Gamma_{n,j}} (\Gamma_{n,j})^k / k! \tag{S13}$$

The evolution is subject to initial condition π_0=[0 0 1 0 ...].

S4 Deterministic recognition dynamics

The intensity parameter in Eqs. S12-S13 under deterministic recognition simplifies to

$$\Gamma_{n,j} = \gamma_{n,j} = j\lambda, \tag{S14}$$

Moreover, if clearance probabilities are homogeneous in time and clone number, $q_n = q_c$, so that the Markov chain in Eq. S12 simplifies to the following homogeneous probability matrix:

$$P = \begin{Vmatrix} 1 & 0 & \cdots & 0 & \cdots \\ 0 & 1 & \cdots & 0 & \cdots \\ 1-q_c & q_c p_0(\lambda) & \cdots & q_c p_2(\lambda) & \cdots \\ 1-q_c^2 & q_c^2 p_0(2\lambda) & \cdots & q_c^2 p_2(2\lambda) & \cdots \\ \vdots & \vdots & \ddots & \vdots & \\ 1-q_c^j & q_c^j p_0(j\lambda) & \cdots & q_c^j p_k(j\lambda) & \cdots \\ \vdots & \vdots & & \vdots & \ddots \end{Vmatrix} \tag{S15}$$

with

$$p_k(j\lambda) = e^{-j\lambda}(j\lambda)^k/k! \tag{S16}$$

and subject to initial condition π_0=[0 0 1 0 ...].

Let $\hat{p}_k^T$ be the k^{th} column vector of P excluding states ∞ and 0, and similarly $\hat{\pi}_n$ be the row vector π_n of states $\{1, 2, \dots\}$. Let $\pi_{n,\infty}$, $\pi_{n,0}$, and $\pi_{n,j}$ denote the probability of escape, elimination, and having j evasive clones at time n, respectively. For this system, we have

$$\pi_{1,\infty} = 1 - q_c, \tag{S17}$$
$$\pi_{1,0} = q_c p_0(\lambda), \tag{S18}$$
$$\pi_{1,j} = q_c p_j(\lambda), \tag{S19}$$

and for $n > 1$,

$$\pi_{n,\infty} = \langle \hat{\pi}_{n-1}, \hat{p}_\infty \rangle + \pi_{n-1,\infty}, \tag{S20}$$
$$\pi_{n,0} = \langle \hat{\pi}_{n-1}, \hat{p}_0 \rangle + \pi_{n-1,0}, \tag{S21}$$
$$\pi_{n,j} = \langle \hat{\pi}_{n-1}, \hat{p}_j \rangle. \tag{S22}$$

where $\langle \cdot, \cdot \rangle$ denotes the usual inner product:

$$\langle x, y \rangle = \sum_{k=1}^{\infty} x_k y_k. \tag{S23}$$

We are primarily interested in characterizing cancer immune escape (resp. clearance) probabilities as a function of clonal branching, given by $\pi_{n,\infty}$ (resp. $\pi_{n,0}$). We calculate the splitting probabilities $\pi_{n,\infty}$ and $\pi_{n,0}$ below. To ease our calculation, we define the following transformation:

$$Tx \equiv q_c e^{-\lambda} e^{-\lambda x}, \tag{S24}$$

where

$$T^n x \equiv \underbrace{T \circ \cdots \circ T}_{n} x. \tag{S25}$$

and $T^0 x = Ix = x$.

We begin by evaluating the inner product in Eq. S20.

$$\begin{aligned}\langle \hat{\pi}_{n-1}, \hat{p}_\infty \rangle &= \sum_{k_n=1}^{\infty} \left(1 - q_c^{k_n}\right) \langle \hat{\pi}_{n-2}, \hat{p}_{k_n} \rangle \\ &= \sum_{k_n=1}^{\infty} \left(1 - q_c^{k_n}\right) \sum_{k_{n-1}=1}^{\infty} p_{k_{n-1},k_n} \hat{\pi}_{n-2,k_{n-1}} \\ &\vdots \\ &= \sum_{k_n=1}^{\infty} \left(1 - q_c^{k_n}\right) \sum_{k_{n-1}=1}^{\infty} p_{k_{n-1},k_n} \sum_{k_{n-2}=1}^{\infty} p_{k_{n-2},k_{n-1}} \cdots \sum_{k_2=1}^{\infty} p_{k_2,k_3} \sum_{k_1=1}^{\infty} p_{k_1,k_2} \pi_{0,k_1}. \end{aligned} \tag{S26}$$

We interchange sums k_n and k_{n-1} under the Fubini-Tonelli Theorem, and expand p_{k_{n-1},k_n}, giving

$$\langle \hat{\pi}_{n-1}, \hat{p}_\infty \rangle = \sum_{k_{n-1}=1}^{\infty} \left(q_c e^{-\lambda}\right)^{k_{n-1}} \sum_{k_n=1}^{\infty} \left[\left(\lambda k_{n-1}\right)^{k_n} - \left(\lambda q_c k_{n-1}\right)^{k_n}\right] \Big/ k_n! \sum_{k_{n-2}=1}^{\infty} p_{k_{n-2},k_{n-1}} \cdots \sum_{k_1=1}^{\infty} p_{k_1,k_2} \pi_{0,k_1}$$

Evaluation of the k_n summand and application of T's definition gives

$$= \sum_{k_{n-1}=1}^{\infty} \left[\left(T^0 q_c\right)^{k_{n-1}} - \left(T q_c\right)^{k_{n-1}}\right] \sum_{k_{n-2}=1}^{\infty} \left(q_c e^{-\lambda}\right)^{k_{n-2}} \left(\lambda k_{n-2}\right)^{k_{n-1}} / k_{n-1}! \cdots \sum_{k_1=1}^{\infty} p_{k_1,k_2} \pi_{0,k_1}$$

Continued iteration ultimately yields

$$\begin{aligned}\langle \hat{\pi}_{n-1}, \hat{p}_\infty \rangle &= \sum_{k_1=1}^{\infty} \pi_{0,k_1} \left[\left(T^{n-2} q_c\right)^{k_1} - \left(T^{n-1} q_c\right)^{k_1}\right] \\ &= T^{n-2} q_c - T^{n-1} q_c. \end{aligned} \tag{S27}$$

Therefore, by Eqs. S20 and S27,

$$\pi_{n,\infty} = \pi_{n-1,\infty} + T^{n-2} q_c - T^{n-1} q_c, \tag{S28}$$

but by the same procedure we also have that

$$\pi_{n-1,\infty} = \pi_{n-2,\infty} + T^{n-3} q_c - T^{n-2} q_c. \tag{S29}$$

Continuing this argument ultimately yields the desired escape probability

$$\begin{aligned}\pi_{n,\infty} &= \pi_{1,\infty} + T^0 q_c - T^{n-1} q_c \\ &= (1 - q_c) + q_c - T^{n-1} q_c \\ &= 1 - T^n 1. \end{aligned} \tag{S30}$$

We take a similar approach to characterize the extinction probability $\pi_{n,0}$ below. Here, we put $x_0 \equiv q_c e^{-\lambda}$.

$$\begin{aligned}\langle \hat{\pi}_{n-1}, \hat{p}_0 \rangle &= \sum_{k_n=1}^{\infty} q_c^{k_n} p_0(\lambda k_n) \pi_{n-1,k_n} \\ &\vdots \\ &= \sum_{k_n=1}^{\infty} q_c^{k_n} p_0(\lambda k_n) \sum_{k_{n-1}=1}^{\infty} p_{k_{n-1},k_n} \sum_{k_{n-2}=1}^{\infty} p_{k_{n-2},k_{n-1}} \cdots \sum_{k_2=1}^{\infty} p_{k_2,k_3} \sum_{k_1=1}^{\infty} p_{k_1,k_2} \pi_{0,k_1}. \end{aligned} \tag{S31}$$

As before, we rearrange and exchange k_n and k_{n-1} sums, replace p_{k_{n-1},k_n} with its value, and evaluate the inner sum, giving,

$$\langle \hat{\pi}_{n-1}, \hat{p}_0 \rangle = \sum_{k_{n-1}=1}^{\infty} \left[\left(q_c e^{-\lambda} e^{\lambda x_0} \right)^{k_{n-1}} - \left(q_c e^{-\lambda} \right)^{k_{n-1}} \right] \sum_{k_{n-2}=1}^{\infty} p_{k_{n-2},k_{n-1}} \cdots \sum_{k_1=1}^{\infty} p_{k_1,k_2} \pi_{0,k_1}$$

Taking an identical approach as in the previous case ultimately gives

$$= T^{n-1} x_0 - T^{n-2} x_0. \tag{S32}$$

Therefore, by Eqs. S21 and S32,

$$\pi_{n,0} = \pi_{n-1,0} + T^{n-1} x_0 - T^{n-2} x_0. \tag{S33}$$

Continued application to $\pi_{n-1,0}$, $\pi_{n-2,0}$, $\ldots$, $\pi_{1,0}$ ultimately gives

$$\pi_{n,0} = T^n 0. \tag{S34}$$

Together, we have at period n the cumulative probability of escape ($\pi_{n,\infty}$), extinction ($\pi_{n,0}$), and progression ($\pi_{n,E}$) to be

$$\pi_{n,0} = T^n 0, \tag{S35}$$
$$\pi_{n,\infty} = 1 - T^n 1, \tag{S36}$$
$$\pi_{n,E} = T^n 1 - T^n 0, \tag{S37}$$

where progression is defined to be any state other than elimination or escape. If $E_n \equiv$ [escape by n], $\tilde{E}_n \equiv$ [escape at n], $F_n \equiv$ [elimination by n], and $\tilde{F}_n \equiv$ [elimination at n], then $\pi_{n,\infty} = \mathbb{P}(E_n)$ and $\pi_{n,0} = \mathbb{P}(F_n)$. Since membership in E_n implies membership in E_{n+1}, we have that $E_n \subset E_{n+1}$ and a similar argument holds for the sequence F_n. The probability that escape and elimination occur at period n are given respectively by

$$\mathbb{P}(\tilde{E}_n) = \mathbb{P}(E_n \setminus E_{n-1}) = \mathbb{P}(E_n) - \mathbb{P}(E_{n-1}) = T^{n-1} 1 - T^n 1, \tag{S38}$$

and similarly,

$$\mathbb{P}(\tilde{F}_n) = T^n 0 - T^{n-1} 0. \tag{S39}$$

S4.1 Branching Process and Probability Generating Functions

S4.1.1 Conditional non-escape

This section details the process assuming non-escape, which is relevant for studying the dynamical transitions prior to escape. If non-escape is guaranteed ($q_c = 1$), then the general framework above reduces to a Poisson Galton-Watson branching process (BP) [2]. In this case, the transformation T above is none other than the probability generating function (pgf) for the progeny of the i^{th} population member at period n, $X_{n,i}$, and is given by

$$G_X(s) = e^{-\lambda(1-s)}, \tag{S40}$$

for $s \in [0, 1]$. Moreover, Z_n evolves according to:

$$Z_0 = 1,$$
$$Z_{n+1} = \sum_{i=1}^{Z_n} X_{n,i}, \tag{S41}$$

and the pgf of Z_{n+1} is the n-fold function composition of G_X

$$G_{Z_n}(s) = \underbrace{G_X \circ \cdots \circ G_X}_{n}(s). \tag{S42}$$

S4.1.2 General case

We generalize the familiar framework above to our process below by augmenting the original sequence of progeny from the i^{th} population at period n, $X_{n,i}$, to a collection, $X_{n,i,j}$, of IID Poisson(λ) random variables, and by introducing an IID collection $Y_{n,i}$ of random variables taking values in $\{1, \infty\}$ so that $\mathbb{P}(Y_{n,i} = 1) = q_c$. Functionally, the $Y_{n,i}$ record the presence or absence of escape of the i^{th} clone at period n. By definition, the probability generating function for the $Y_{n,i}$ is given by

$$G_Y(s) = q_c s + \lim_{z\to\infty}(1 - q_c)s^z. \tag{S43}$$

We relate Z_{n+1} to Z_n via the $Y_{n,i}$ and $X_{n,i,j}$ below. If any of the time-n clones escape, then $Z_{n+1} = \infty$. If on the other hand all of the clones are cleared, then Z_{n+1} is the usual sum above. We adopt the convention that $0 \cdot \infty = 0$. The process evolves according to:

$$\begin{aligned} Z_0 &= 1 \\ Z_{n+1} &= \left\{ \begin{array}{cc} \infty, & Y_{n,i} = \infty \text{ for some } i \in \{1, \ldots, Z_n\} \\ \sum_{i=1}^{Z_n} X_{n,i}, & Y_{n,i} = 1 \text{ for all } i \in \{1, \ldots, Z_n\} \end{array} \right\} = \sum_{i=1}^{Z_n} \big[(Y_{n,i} - 1) + Y_{n,i}X_{n,i,1}\big]. \end{aligned} \tag{S44}$$

With some partitioning and re-arranging, we find that

$$\begin{aligned} Z_{n+1} &= \sum_{i=1}^{Z_n} Y_{n,i}X_{n,i,1}I_{[Y_{n,i}=1]} + \sum_{i=1}^{Z_n} \big[Y_{n,i}(1 + X_{n,i,1}) - 1\big]I_{[Y_{n,i}=\infty]} \\ &= \sum_{i=1}^{Z_n}\sum_{j=1}^{Y_{n,i}} X_{n,i,j}I_{[Y_{n,i}=1]} + \sum_{i=1}^{Z_n} Y_{n,i}(1 + X_{n,i,1})I_{[Y_{n,i}=\infty]}, \end{aligned} \tag{S45}$$

where

$$I_E(\omega) = \left\{ \begin{array}{ll} 1, & \omega \in E; \\ 0, & \omega \notin E. \end{array} \right. \tag{S46}$$

We observe that for the event $E_j \equiv [X_{n,i,j} \geq 1]$ we have that $\mathbb{P}(E_j) = 1 - e^{-\lambda}$ so that $\sum_{j=1}^{k}\mathbb{P}(E_j) \to \infty$ as $k \to \infty$. Thus, by the Borel-Cantelli lemma, elements of $\{X_{n,i,j}\}_{j=1}^{\infty}$ attain a value of at least one infinitely often, so that $\sum_{j=1}^{k} X_{n,i,j} \to Y_{n,i}(1 + X_{n,i,j})$ almost surely (a.s.) as $k \to \infty$ on $[Y_{n,i} = \infty]$. Thus,

$$Y_{n,i}(1 + X_{n,i,1})I_{[Y_{n,i}=\infty]} \overset{\text{a.s.}}{=} \lim_{k\to\infty}\sum_{j=1}^{k} X_{n,i,j}I_{[Y_{n,i}=\infty]} = \sum_{j=1}^{Y_{n,i}} X_{n,i,j}I_{[Y_{n,i}=\infty]}, \tag{S47}$$

and so by Eq. S45 the dynamics may be re-written as

$$\begin{aligned} Z_0 &= 1, \\ Z_{n+1} &\overset{\text{a.s.}}{=} \sum_{i=1}^{Z_n}\sum_{j=1}^{Y_{n,i}} X_{n,i,j}. \end{aligned} \tag{S48}$$

The reduced representation above represents the current model as an extension of the usual branching process theory. This motivates the interpretation that general recognition may be viewed as a straightforward sum of IID Poisson replicates if all clones are controlled. If on the other hand at least one clone escapes, then the subsequent sum contains at least one collection of infinite IID Poisson random variates, which is infinite with probability one. This representation reveals how G relates to T. We define the compound pgf

$$G_Z(s) \equiv G_Y \circ G_X(s) = q_c e^{-\lambda(1-s)} + (1 - q_c)\lim_{z\to\infty} e^{-\lambda(1-s)z} = \left\{ \begin{array}{cc} Ts, & s \in [0, 1); \\ 1, & s = 1. \end{array} \right. \tag{S49}$$

And thus, G_{Z_n} may be solved iteratively by the following:

$$G_{Z_n}(s) = G_{Z_{n-1}} \circ G_Z(s) = ... = \underbrace{G_Z \circ \cdots \circ G_Z}_{n}(s). \tag{S50}$$

This alternative interpretation will be used to greatly simplify the more complicated derivation for the adaptive case. We note that $G_Z(\cdot)$ and $T(\cdot)$ agree except when evaluated at 1.

S4.2 Limiting Distribution

Extinction and escape clearly depend on the transformation $Tx = q_c e^{-\lambda(1-x)}$. We now consider limiting behavior for $\pi_{n,\infty}$ and $\pi_{n,0}$. We recall that $x, q_c \in [0,1]$ and $\lambda > 0$.

If $q_c = 0$, then $Tx = 0$ for each x so that $\pi_{n,\infty} = 1$ and $\pi_{n,0} = 0$ for $n > 0$ and in this case escape is certain. If $q_c = 1$, then $Tx = e^{-\lambda(1-x)}$ so that $T1 = 1$, and so $\pi_{n,\infty} = 0$ for $n \geq 0$. In this case, which we discuss in Section S4.3, immune escape never occurs as each new clone is cleared. Arguably the most interesting case is when $q_c \in (0,1)$ so that clearance is neither guaranteed nor impossible. We consider the sequence $x_n = T^n x_0$ for $n \geq 1$. If $x_n < x_{n-1}$ then

$$x_{n+1} = q_c e^{-\lambda} e^{\lambda x_n} < q_c e^{-\lambda} e^{\lambda x_{k-1}} = x_n. \tag{S51}$$

A similar argument shows that $x_n > x_{n-1}$ implies that $x_{n+1} > x_n$. This, together with the fact that $0 < T0 = q_c e^{-\lambda} < q_c = T1 < 1$ implies that $\{\pi_{n,0}\}_n$ and $\{\pi_{n,\infty}\}_n$ are both increasing sequences. It can be shown that T admits a unique fixed point, p^*, by the contraction mapping theorem, given by

$$p^* = -\lambda^{-1} W\big(-\lambda q_c e^{-\lambda}\big), \tag{S52}$$

where W is the Lambert W function, defined as the inverse function

$$W(xe^x) \equiv f^{-1}(xe^x) = x, \tag{S53}$$

with a lower branch domain of $[-1/e, 0]$ from $W(-1/e) = -1, W(0) = 0$. We thus have

$$\pi_{n,\infty} = 1 - T^n 1 \to 1 - p^* \quad \text{as } n \to \infty; \tag{S54}$$

$$\pi_{n,0} = T^n 0 \to p^* \quad \text{as } n \to \infty; \tag{S55}$$

$$\pi_{n,E} = T^n 1 - T^n 0 \to 0 \quad \text{as } n \to \infty. \tag{S56}$$

Thus, in this case, progression after a long time is impossible. Simulation results for a finite number of steps agree with this analytic characterization, with convergence observed for super-critical and sub-critical cases (Fig. 3A-B). The limiting extinction probability p^* is plotted as a function of normalized net growth rate and clearance probability in Fig. 3C, assuming detection limited by total net growth rate [1]. This process exhibits sneak-through, wherein, all else equal, slow-growth threats have an advantage at avoiding extinction over their faster growing counterparts, consistent with earlier modeling efforts and empirical observation. When it comes to escape, intermediate-growth threats are at a disadvantage due to reductions in λ_0 relative to their faster and slower growing counterparts.

If in addition $q_c \to 1$ (guaranteed non-escape) and $\lambda \leq 1$ (average production does not exceed more than one clone per recognition cycle), then

$$p^* = -\lambda^{-1} W(-\lambda e^{-\lambda}) = -\lambda^{-1}(-\lambda) = 1, \tag{S57}$$

since for the lower branch $W(xe^x) = x$ for $x \leq 1$ and so extinction occurs with certainty. Alternatively, if either $q_c = 0$ or $\lambda = 0$, then $p^* = 0$ escape occurs with certainty.

S4.3 Stable equilibrium

This section briefly discusses the possibility of obtaining stable equilibrium. In particular, we are interested in characterizing the time-homogeneous condition on clearance probabilities that allows for a state of non-escape, non-elimination with some positive probability. We are motivated by the observation that adaptive immunity has been implicated in maintaining occult cancer in an equilibrium state [6], and these empirical observations distinguish equilibrium from tumor elimination and escape. Technically speaking, equilibrium states are those that occur with nonzero probability in the long time limit. In particular, the case above does not permit any other equilibrium states since

$$\lim_{n\to\infty} \pi_{n,0} + \pi_{n,\infty} = p^* + (1 - p^*) = 1. \tag{S58}$$

If optimistically $q_c = 1$, we obtain a standard Galton-Watson branching process with the limiting escape and elimination probabilities determined solely by λ [2]. In particular, $\lambda < 1$ and $\lambda = 1$ correspond to the sub-critical and critical processes wherein ultimate extinction is certain, and therefore ultimate equilibrium is impossible.

If however we restrict our attention to the case with $\lambda > 1$ corresponding to net expansion of clones over the recognition cycles, and relax the assumption on per-clone clearance rate, we find that ultimate equilibrium values are attainable. We previously assumed that the per-clone clearance rate $q_{n,i} = q_c < 1$ was fixed. In this case, the escape probability $p_{esc} = 1 - q_c^j \to 1$ as $j \to \infty$ so that escape is certain for arbitrarily large clone sizes, implying again that ultimate equilibrium does not occur with probability one. Relaxing the constitutive form of clearance probabilities q_c to allow for differences in targeting based on an ordering of the current clones $q_i = q_{c,i}$ so that clearance probabilities may be inhomogeneous in clone-size makes it possible. In this case, the generalized Markov chain from Eq. S12 becomes

$$P_n = \begin{array}{c|cccccc} & \boldsymbol{\infty} & \mathbf{0} & \mathbf{1} & \cdots & \boldsymbol{k} & \cdots \\ \hline \boldsymbol{\infty} & 1 & 0 & 0 & \cdots & 0 & \cdots \\ \mathbf{0} & 0 & 1 & 0 & \cdots & 0 & \cdots \\ \mathbf{1} & 1-q_{n,1} & q_{n,1}p_0(\Gamma_{n,1}) & q_{n,1}p_1(\Gamma_{n,1}) & \cdots & q_{n,1}p_k(\Gamma_{n,1}) & \cdots \\ \mathbf{2} & 1-q_{n,1}q_{n,2} & q_{n,1}q_{n,2}p_0(\Gamma_{n,2}) & q_{n,1}q_{n,2}p_1(\Gamma_{n,2}) & \cdots & q_{n,1}q_{n,2}p_k(\Gamma_{n,2}) & \cdots \\ \vdots & \vdots & \vdots & \vdots & \ddots & \vdots & \\ \boldsymbol{j} & 1-\prod_{i=1}^{j} q_{n,i} & p_0(\Gamma_{n,j})\prod_{i=1}^{j} q_{n,i} & p_1(\Gamma_{n,j})\prod_{i=1}^{j} q_{n,i} & \cdots & p_k(\Gamma_{n,j})\prod_{i=1}^{j} q_{n,i} & \cdots \\ \vdots & \vdots & \vdots & \vdots & & \vdots & \ddots \end{array} \tag{S59}$$

with

$$p_{esc} = 1 - \prod_{i=1}^{j} q_{c,i} \tag{S60}$$

We assume monotonicity in $\{q_{c,i}\}_i$, so that additional threats either encourage or hinder immune recognition. If $\{q_{c,i}\}_i$ is non-increasing, then $p_{esc} \leq 1 - q_{c,0}^j \to 1$ as $j \to \infty$. Ultimate equilibrium may be achieved if $q_{c,i}$ increases quickly enough. For example, if $q_{c,i} = a_i/a_{i-1}$ for $a_i \equiv 1 + \delta/2$ and $\delta > 0$ then $\{q_{c,i}\}_{i=1}^{\infty} < 1$ is an increasing sequence. Moreover, $\prod_{i=1}^{j} q_{c,i} = a_j/a_0 \to 1/(1+\delta)$ as $j \to \infty$. Thus escape occurs with probability $p_{esc} \to \delta/(\delta+1)$. If in addition $\lambda > 1$, ultimate extinction is also not guaranteed, so that non-escape and non-extinction may co-exist.

In summary, under most cases, ultimate equilibrium is not predicted. If there is net expansion $\lambda > 1$ and the immune system is on heightened alert to keep up with increasing clone sizes by increasing $p_{c,i}$ at sufficient rates for increasing i, then in theory this is possible. not only must clearance probabilities approach

unity as an increasing number of clones are produced, they must do so sufficiently quickly. Though difficult to determine experimentally, such an ultimate equilibrium seems an exceedingly unlikely approximation to reality from our findings, since the number of total tumor cells $m_0 X$ scales as the number of immunologically distinct clones X grows arbitrarily large. Additionally, evidence of immunodominance is more consistent with immune decline, not enhancement, as increasing numbers of distinct clones are encountered under normal conditions [8].

S4.4 Inter-temporal immune decline

Here we consider temporally decreasing clearance probabilities. This can be viewed as an extension to our earlier work [1] wherein immune surveillance occurs over a single generation and the current clone either became recognized or escaped via acquisition of a single, completely evasive phenotype. Our earlier characterization represents an extreme case where a single event imparts complete and lasting immune evasion and is easily modeled in the above framework by taking $q_{0,1} = q_c$ and $q_n = 0$. This is in contrast to the modeling effort in Secs. S4.1-S4.2 which may be viewed as the opposite extreme wherein, for each period, the immune system is equally capable of recognizing threats in an identical manner *ad infinitum* until either one clone escapes or the entire population becomes extinct. For the intermediate case, we assume that $q_n = f(q_c, n)$ is a (known) decreasing sequence of clearance probabilities with maximal clearance $q_c \equiv q_0$. For analytic comparison, we consider the truncated sequence for $q_c > 0$, $N > 0$ such that

$$q_n = \begin{cases} f(q_c, n), & n \leq N; \\ 0, & n > N. \end{cases} \tag{S61}$$

Of course, $q_n \to f(q_c, n)$ as $N \to \infty$. By repeating an approach similar to that of Eq. S26, we may obtain

$$\pi_{n,\infty} = 1 - \big(T_1 \circ T_2 \circ \cdots \circ T_n\big)\big(1\big), \tag{S62}$$

$$\pi_{n,0} = \big(T_1 \circ T_2 \circ \cdots \circ T_n\big)\big(0\big). \tag{S63}$$

Agreement between the analytical theory and simulations are given in Fig. S2. Fig. S2A provides an example where $f(q_c, n) \to 0$ as $n \to \infty$. in Fig. S2B, $f(q_c, n) \to 1/2$ as $n \to \infty$. In any case, decreasing f implies no equilibrium state aside from escape or elimination.

S4.5 Clone frequency-dependent recognition

It is also reasonable to assume that the clearance probability for a given clone decreases as the number of total clones (and hence population members) increase, and we briefly provide an estimate of this behavior for comparison to the prior inhomogeneous case. If there are j clones at time step n, each having population size m_j, and we assume that the clearance probability scales inversely with population size, then the clearance probability of the k^{th} clone at period n is

$$q_{n,k} = q_c m_k / \sum_{i=1}^{j} m_i, \tag{S64}$$

assuming a maximal recognition probability of q_c when there are no competing cones. Under deterministic recognition $m_k = m_0$ and $m_i \leq m_0$. This gives the following lower-estimate on clearance probability

$$q_{n.k} \geq q_c m_k / (j m_0) \tag{S65}$$

giving

$$q_{n,j} \simeq q_c / j. \tag{S66}$$

A comparison between escape probabilities for the constant and declining clearance probability assumptions is given in Figure S3. As expected, declining clearance results in increased rates of threat escape in both supercritical and subcritical regimes.

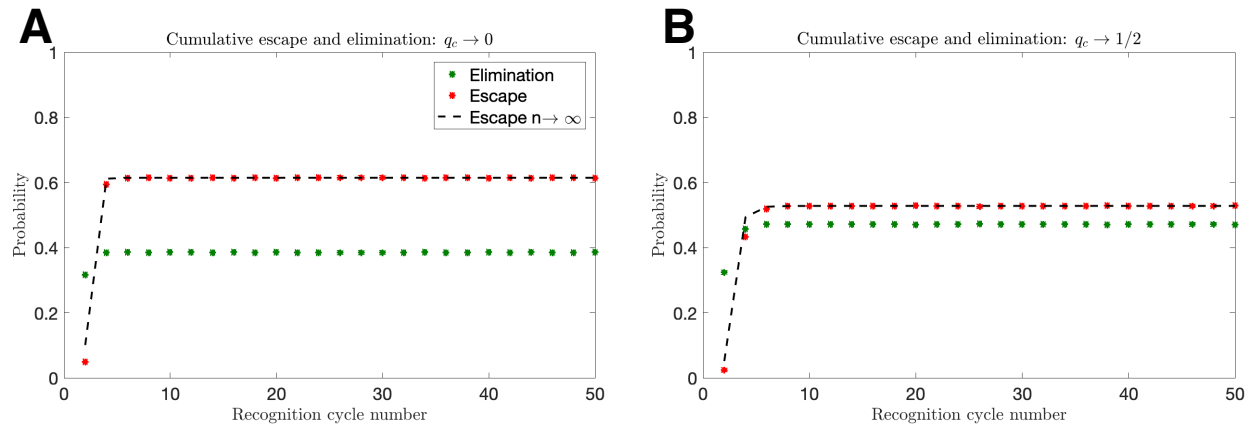

Figure S2: Escape and elimination probabilities with variable clearance. The probability of elimination (red) and escape (blue) are simulated for variable decreasing immune profiles $f(q_c, n)$ (A) $f(q_c, n) = q_c/n$, (B) $f(q_c, n) = (q_c + n)/2n$. Escape values are compared to the analytical result of Eq. S62 (dashed line). (In each case, $q_c = 0.95$; net growth is assumed with $\lambda = 1.1$; simulations averaged over 10^6 iterations.)

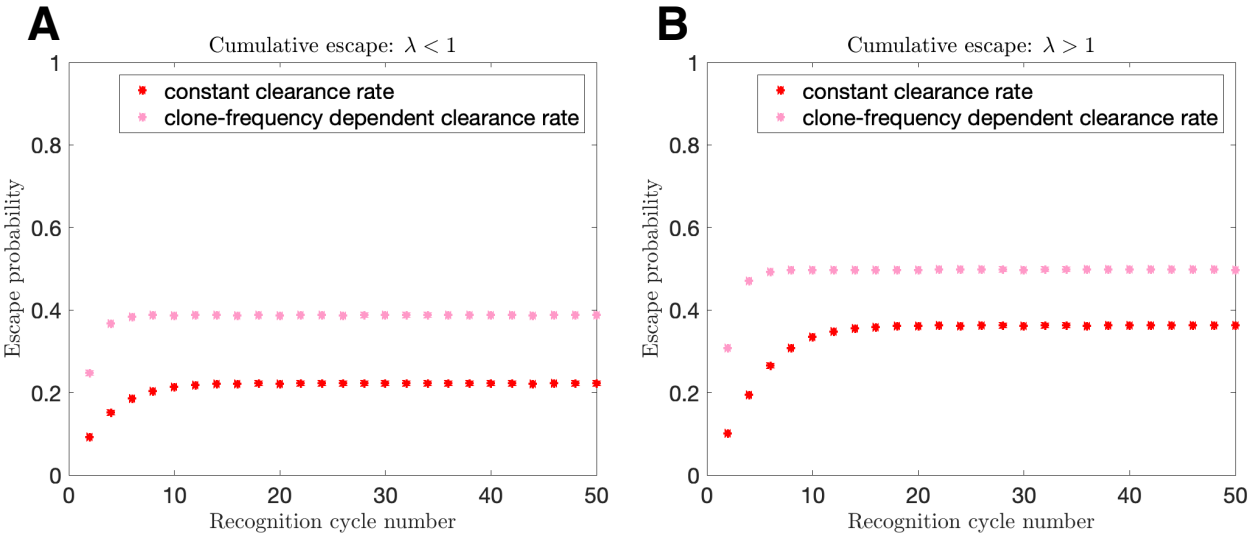

Figure S3: Enhancement in escape with frequency-dependent declines in clearance probability. Escape probabilities assuming clearance probabilites with constant ($q_{n,j} = q_c$; red) and clone-dependent declines ($q_{n,j} = q_c/j$; pink) are given assuming deterministic recognition for (A) supercritical ($\lambda = 1.1$) and (B) subcritical ($\lambda = 0.9$) branching. (Results averaged across 10^6 iterations for each case.)

S5 Adaptive recognition dynamics

In this section we investigate the more general problem where individual clones may be recognized at different sizes, allowing a variety of subsequent daughter clone arrival rates depending on the particular clone and recognition cycle number. This is complicated for general recognition distributions on $\{m_0, m_0+1, \dots\}$. Below, we outline a particular case where a reasonable distribution is assumed, under recognition rates that are homogeneous in time and across clones.

The clone size in the deterministic case was represented by the sum of $Y_{n,i}$ total IID Poisson random variables $X_{n,i,j}$, for each clone present at time n (Eq. S48). In the adaptive case, additional clones may arrive from the i^{th} population by virtue of the fact that they need not be recognized at minimal size m_0. Arrival rates therefore can be represented by a base rate $\lambda_0 m_0$ plus an additional rate that depends on the random size at immune detection. We construct this rate below by assuming that the average number of new clones generated from the ith clone at period n, given by $\Lambda_{n,i}$ is in general of the form

$$\Lambda_{n,i} = a\tilde{Y}_{n,i} + b, \tag{S67}$$

where b represents the base arrival rate at minimal detection size m_0, and $\tilde{Y}_{n,i} \sim \text{Poisson}(\nu)$ is an IID collection of random variables representing the additional rate in the adaptive case owing to possible stochastic recognition above detection size. $\Lambda_{n,i}$ has support

$$\Lambda_{n,i} \in \{b+a, b+2a, b+3a, \dots\}. \tag{S68}$$

The IID requirement imposed on the $\tilde{Y}_{n,i}$ means that the distribution of rates for new clone arrivals are homogeneous in clone number and time. More generally, the $\tilde{Y}_{n,i}$ can take any reasonable (i.e. integrable) distribution characterizing arrival probabilities. We will see that when they are Poisson distributed we recover homogeneity of the Markov chain. The parameter $\nu \geq 0$ inversely relates with general immune functioning. Intrinsic and extrinsic immuno-modulation that results in decreased adaptive immune functioning is modeled by increasing ν. This generalizes the previous framework where $\nu = 0$. $\Lambda_{n,i}$ is analogous to λ in the deterministic recognition case, and the corresponding intensity of new clone arrivals for j distinct clones in this setting is given by

$$\Gamma_{n,j} = \sum_{i=1}^{j} \Lambda_{n,i} = a\sum_{i=1}^{j} \tilde{Y}_{n,i} + jb, \tag{S69}$$

which is the adaptive analogue of the deterministic intensity $\gamma_{n,j} = j\lambda$ (Eq. S6). By construction, $\Gamma_{n,j} \sim \text{Poisson}(j\nu)$ having support

$$\Gamma_{n,j} \in \{jb, a+jb, 2a+jb, 3a+jb, \dots\} \tag{S70}$$

so that for $\alpha_\ell \equiv jb + a\ell$,

$$\begin{aligned} m_j(\ell) \equiv \mathbb{P}\big(\Gamma_{n,j} = \alpha_\ell\big) &= e^{-j\nu}\big(j\nu\big)^{(\alpha_\ell - jb)/a} \Big/ \Big(\frac{\alpha_\ell - jb}{a}\Big)! \\ &= e^{-j\nu}\big(j\nu\big)^{\ell}/\ell! \end{aligned} \tag{S71}$$

The above framework generalizes deterministic recognition, which is obtained by setting $a = 0$ and $b = \lambda$ so that probability mass one is assigned to $\Lambda_{n,i} = \lambda$ and $\Gamma_{n,j} = j\lambda$. However, for adaptive recognition the desired parameter selection is $a = \lambda_0$ and $b = \lambda$, so that

$$\Lambda_{n,i} = \lambda_0\tilde{Y}_{n,i} + \lambda, \tag{S72}$$

and $\Gamma_{n,j}$ has support

$$\Gamma_{n,j} \in \{\lambda, \lambda+\lambda_0, \lambda+2\lambda_0, \dots\} = \{\lambda_0 m_0, \lambda_0(m_0+1), \lambda_0(m_0+2), \dots\}. \tag{S73}$$

This represents well the distribution of intensities as a function of random recognition sizes in the limit of large terminal population limit $M \gg m_0$ [1].

The deterministic analogue to $\Gamma_{n,j}$, the clone generation intensity at period n when there are j current clones, is fixed at $\gamma_{n,j}$, so clearly,

$$\mathbb{E}[\gamma_{n,j}] = \lambda j; \qquad \mathrm{Var}\big(\gamma_{n,j}\big) = 0, \tag{S74}$$

follows directly by definition. We introduce $W_{n,j} = \sum_{i=1}^{j} \tilde{Y}_{n,i} \sim \mathrm{Poisson}(j\nu)$ to characterize the adaptive case. Here, the expected clone intensity is

$$\mathbb{E}\big[\Gamma_{n,j}\big] = \lambda j + \lambda_0 \mathbb{E}\big[W_{n,j}\big] = (\lambda + \lambda_0 \nu) j. \tag{S75}$$

Its second moment is

$$\mathbb{E}\big[\Gamma_{n,j}^2\big] = \mathbb{E}\big[\big(\lambda j + \lambda_0 W_{n,j}\big)^2\big] = (\lambda j)^2 + 2\lambda_0 \lambda \nu + \lambda_0^2 \mathbb{E}\big[W_{n,j}^2\big]. \tag{S76}$$

Since, $W_{n,j} \sim \mathrm{Poisson}(j\lambda)$, we have that

$$\mathbb{E}\big[W_{n,j}^2\big] = \mathrm{Var}\big(W_{n,j}\big) + \mathbb{E}\big[W_{n,j}\big]^2 = \lambda j + (\lambda j)^2. \tag{S77}$$

Together, we have that

$$\mathrm{Var}\big(\Gamma_{n,j}\big) = \lambda_0^2 \nu j. \tag{S78}$$

In the deterministic case, the per-clone generation intensity, or branching parameter λ, is fixed and scales linearly with the total number of current clones. This contrasts with the adaptive case where the branching parameter, $\tilde{\lambda}$, is a random variable with a mean always in excess of the deterministic value by an amount equal to the product of per-cell intensity and detection variability (e.g. $\lambda_0 \nu$), so that

$$\tilde{\lambda} = \lambda + \lambda_0 \nu. \tag{S79}$$

Moreover, the variance in intensity scales linearly with the total clone number.

As before, we assume for simplicity that clearance probabilities $q_n = q_c$ are homogeneous across generational periods. Let $\pi_{n,k}$ represent the probability of having k evasive clones after n recognition cycles. In this case, Eq. S12 becomes

$$\tilde{P}_n = \begin{Vmatrix} 1 & 0 & 0 & \cdots & 0 & \cdots \\ 0 & 1 & 0 & \cdots & 0 & \cdots \\ 1-q_c & q_c p_0(\Gamma_{n,1}) & q_c p_1(\Gamma_{n,1}) & \cdots & q_c p_k(\Gamma_{n,1}) & \cdots \\ 1-q_c^2 & q_c^2 p_0(\Gamma_{n,2}) & q_c^2 p_1(\Gamma_{n,2}) & \cdots & q_c^2 p_k(\Gamma_{n,2}) & \cdots \\ \vdots & \vdots & \vdots & \ddots & \vdots & \\ 1-q_c^j & q_c^j p_0(\Gamma_{n,j}) & q_c^j p_1(\Gamma_{n,j}) & \cdots & q_c^j p_k(\Gamma_{n,j}) & \cdots \\ \vdots & \vdots & \vdots & & \vdots & \ddots \end{Vmatrix} \tag{S80}$$

with $0 \le p_c \le 1$ fixed, $\Gamma_{n,j} \sim \mathrm{Poisson}\big(j\nu\big)$, and

$$p_k(\Gamma_{n,j}) = e^{-\Gamma_{n,j}} (\Gamma_{n,j})^k / k! \tag{S81}$$

subject to initial condition π_0=[0 0 1 0 ...].

Instead of guessing the proper transformation relating to splitting probabilities, we will use the BP interpretation from Sec. S4.1 to easily obtain the corresponding PGF and transformation for the adaptive case.

S5.1 Branching Process and Probability Generating Functions

We characterize adaptive recognition dynamics as a branching process as we did in the deterministic case. Below, we will distinguish elements unique to the adaptive case from the deterministic case by use of a tilde. For example, $\tilde{Z}_n$ is the clone number at time n under the adaptive detection assumption. The adaptive dynamics take the following form:

$$\begin{aligned}\tilde{Z}_0 &= 1,\\ \tilde{Z}_{n+1} &= \sum_{i=1}^{\tilde{Z}_n}\left[\sum_{j=1}^{Y_{n,i}} X_{n,i,j} + \sum_{j=1}^{\tilde{Y}_{n,i}} \tilde{X}_{n,i,j}\right].\end{aligned} \tag{S82}$$

This quantity differs from Eq. S48 by the addition of a second term. The $\tilde{X}_{n,i,j} \sim \text{Poisson}(\lambda_0)$ represent additional clone arrivals from clone i at time n for each population size in excess of detection size m_0, and $\tilde{Y}_{n,i} \sim \text{Poisson}(\nu)$ represents the (random) size at which clone i is detected at time n. The pgfs of the new random variables are given by

$$G_{\tilde{X}}(s) = e^{-\lambda_0(1-s)}, \tag{S83}$$

$$G_{\tilde{Y}}(s) = e^{-\nu(1-s)}. \tag{S84}$$

The above representation allows for straightforward characterization of the overall pgf, given by

$$G_{\tilde{Z}_n}(s) = \underbrace{G_{\tilde{Z}} \circ \cdots \circ G_{\tilde{Z}}}_{n}(s), \tag{S85}$$

with

$$G_{\tilde{Z}}(s) = \big(G_Y \circ G_X\big) \cdot \big(G_{\tilde{Y}} \circ G_{\tilde{X}}\big)(s) = G_Z(s) e^{-\nu\left[1-e^{-\lambda_0(1-s)}\right]} \tag{S86}$$

related to the adaptive case via $G_Z(s)$ in Eq. S49. The corresponding transformation is given by

$$\tilde{T}x \equiv q_c e^{-\lambda(1-x)-\nu\left(1-e^{-\lambda_0(1-x)}\right)} \tag{S87}$$

It can be shown, employing a similar strategy as in the deterministic case, that the above transformation can be used to organize the extinction and elimination probabilities. In this case,

$$\tilde{\pi}_{n,\infty} = 1 - \tilde{T}^n 1, \tag{S88}$$

$$\tilde{\pi}_{n,0} = \tilde{T}^n 0, \tag{S89}$$

$$\tilde{\pi}_{n,E} = \tilde{T}^n 1 - \tilde{T}^n 0. \tag{S90}$$

S5.1.1 Conditional non-escape

The process transitions via progression until an escape or evasion event finally occurs. This section considers simplified dynamics assuming that escape does not occur under adaptive recognition (in a similar manner to Sec. S4.1.1). Here we have the Galton-Watson pgf for when non-escape is guaranteed ($q_c = 1$):

$$G_{\tilde{Z}}(s) = e^{-\lambda_0 m_0(1-s)-\nu\left[1-e^{-\lambda_0(1-s)}\right]} \tag{S91}$$

with

$$\frac{\partial G_{\tilde{Z}}}{\partial s} = \lambda_0\left[m_0 + \nu e^{-\lambda_0(1-s)}\right]G \tag{S92}$$

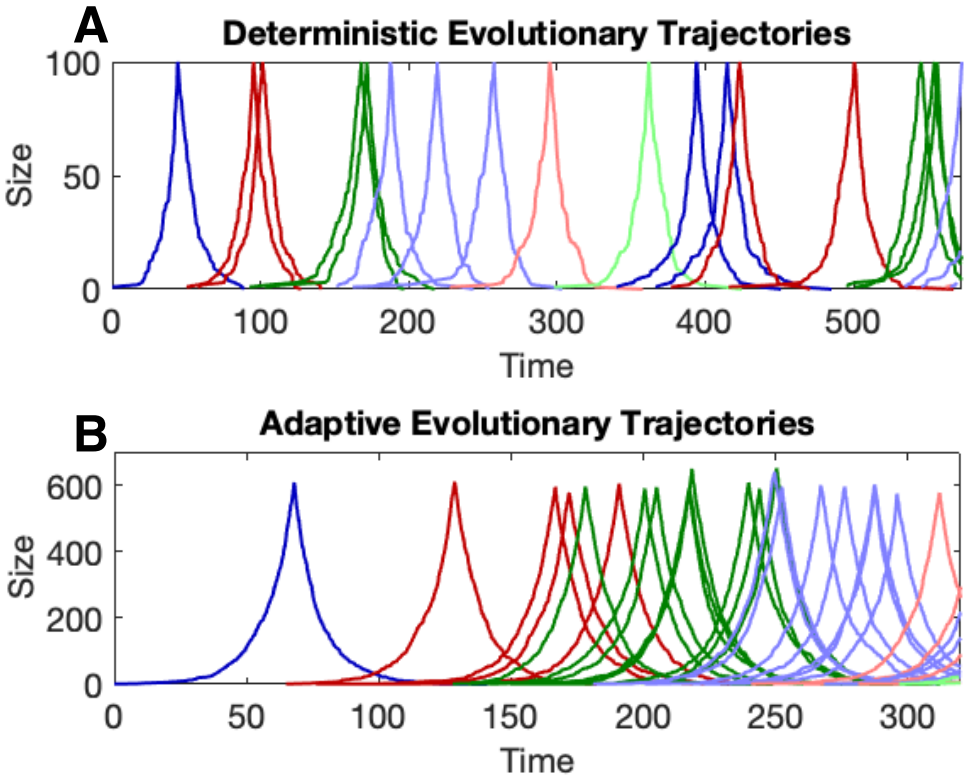

Figure S4: Population dynamics. Evolutionary recognition trajectories under (A) deterministic recognition and (B) adaptive recognition ($\nu = 500$). Escape values are compared to the analytical result of Eq. S62 (dashed line). For both cases, ultimate escape occurs (escape trajectories not illustrated past m_0), and colors distinguish clones arriving across each time period (In each case, $q_c = 0.95$; $r = 0.1$, $d = 0.2$, $m0 = 100$, μ chosen so that the expected number of progeny per clone, λ or $\tilde{\lambda}$, is 1.1).

and

$$\frac{\partial^2 G_{\tilde{Z}}}{\partial s^2} = \lambda_0^2\left[m_0 + \nu e^{-\lambda_0(1-s)}\right]^2 G + \lambda_0\left[\nu e^{-\lambda_0(1-s)}\right]^2 G \tag{S93}$$

which is used to calculate the mean number of clones generated from a single population. Of course, the mean should agree with the process branching parameter:

$$\mathbb{E}\left[\tilde{Z}\right] = G'(1-) = \lambda_0(m_0 + \nu) = \tilde{\lambda}. \tag{S94}$$

The variance is given by

$$\begin{aligned}\tilde{\sigma} \equiv \mathrm{Var}\left(\tilde{Z}\right) &= G''(1-) + G'(1-) - G'(1)^2 \\ &= \lambda_0(m_0 + \nu) + \lambda_0^2\nu \\ &= \tilde{\lambda} + \lambda_0^2\nu.\end{aligned} \tag{S95}$$

Branching process theory [2] enables mean-variance analysis of $\tilde{Z}_n$. In particular, for $\tilde{\lambda}_n \equiv \mathbb{E}\left[\tilde{Z}_n\right]$, and $\tilde{\sigma}_n^2 \equiv \mathrm{Var}\left(\tilde{Z}_n\right)$, we have

$$\tilde{\lambda}_n = \tilde{\lambda}^n \tag{S96}$$

and

$$\tilde{\sigma}_n^2 = \begin{cases} \tilde{\lambda}^{n-1}\tilde{\sigma}^2\left(\dfrac{1-\tilde{\lambda}^n}{1-\tilde{\lambda}}\right), & \tilde{\lambda} \neq 1; \\ n\tilde{\sigma}^2, & \tilde{\lambda} = 1. \end{cases} \tag{S97}$$

We remark that the deterministic case takes the same form, replacing $\tilde{\lambda}$ with λ and $\tilde{\sigma}^2$ with σ^2.

S5.2 Limiting Distribution

We denote by $Sx \equiv \exp\{-\nu[1-e^{-\lambda_0}]\} \leq 1$ so that $\tilde{T} = TS$. continuity of T, S implies that $\tilde{T}x - x$ is continuous with $\tilde{T}1 - 1 < 0 < \tilde{T}0 - 0$. The existence of a fixed point $\tilde{p}^*$ of $\tilde{T}$ follows from the mean value theorem. Explicit values for $\tilde{p}^*$ may be solved for numerically. We note that, as with T, a similar approach shows that for $\tilde{x}_n \equiv \tilde{T}^n\tilde{x}$, we have that $\tilde{x}_{n-1} < \tilde{x}_n \Rightarrow \tilde{x}_n < \tilde{x}_{n+1}$ as well as $\tilde{x}_{n-1} > \tilde{x}_n \Rightarrow \tilde{x}_n > \tilde{x}_{n+1}$. This, together with the fact that $\tilde{T}p^* = Tp^*Sp^* \leq Tp^*$, implies that $\tilde{p}^* < p^*$ for all relevant parameterizations. Since in both cases, the fixed point represents the limiting probability of extinction, this relation agrees with the expectation that ultimate elimination should be greater in the case of deterministic recognition.

S6 Clinical escape

The prior sections detailed escape and elimination probabilities for the deterministic and adaptive cases. In this section, we discuss an extension of the model that accounts for observable clonal behavior that arises post-escape or elimination. We denote by $\hat{Z}_n$ the process that is allowed to progress up to immune escape, assuming adaptive recognition. Let τ_∞ denote the random time of escape (of course, the population becomes extinct at elimination time τ_0). We may write this time as

$$\tau_\infty = \min_n \left\{ n \ : \ Y_{n-1,i} = \infty, \ \ \exists i, \ 1 \leq i \leq \hat{Z}_{n-1} \right\}. \tag{S98}$$

If escape occurs at time τ_∞, then a subset, N, of the Z_{τ_∞} of clones escape. If we assume that an escaping clone has a finite capacity to develop new clones before being detected at some upper size M, then such a clone generates progeny clones with intensity $\lambda_\infty = \mu M$. We introduce the collection of IID random variables $\hat{X}_{n,i} \sim \text{Poisson}(\lambda_\infty)$. If we further order the $\hat{Z}_{\tau_\infty - 1}$ starting with the escaping clones, then we may write

$$\hat{Z}_{n+1} = \sum_{i=1}^{\hat{Z}_n} \left[X_{n,i} + \sum_{j=1}^{\tilde{Y}_{n,i}} \tilde{X}_{n,i,j} \right], \qquad\qquad n < \tau_\infty; \tag{S99}$$

and

$$\hat{Z}_{\tau_\infty+1} = \sum_{i=N+1}^{\hat{Z}_{\tau_\infty}} \left[X_{\tau_\infty,i} + \sum_{j=1}^{\tilde{Y}_{\tau_\infty,i}} \tilde{X}_{\tau_\infty,i,j} \right] + \sum_{i=1}^{N} \hat{X}_{n,i}, \qquad n = \tau_\infty < \tau_0. \tag{S100}$$

where $\hat{X}_{n,i}$, representing the number of new progeny due to an escaping clone, are Poisson-distributed random variables with intensity λ_∞. The stopped process is given by

$$\hat{Z}_{\min\{n,\tau_0,\tau_\infty\}}. \tag{S101}$$

We also allow for a distinct clearance probability during escape, denoted $q_{c,\infty}$. Of course, if each clone has an independent probability of escaping, then the number of sub-clones generated by an escaping clone, N, is described by

$$N \sim \text{Binomial}(Z_{\tau_\infty}, 1 - p_{c,\infty}). \tag{S102}$$

Fig. S5 provides an example of clinical escape dynamics.

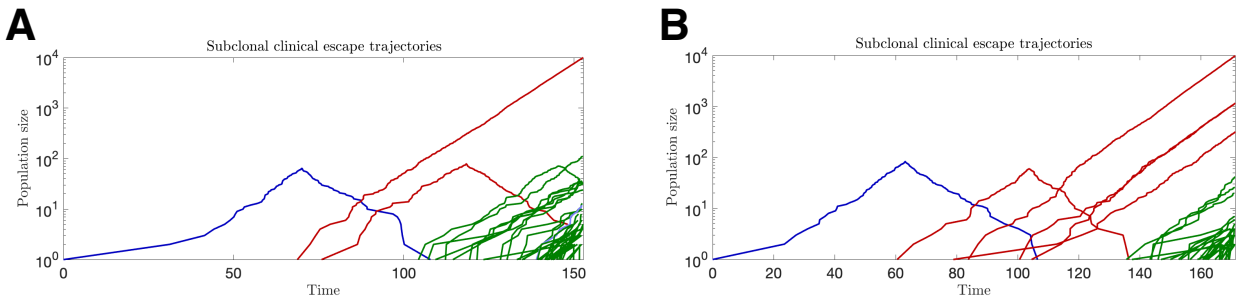

Figure S5: Dynamics of Escape. (A-B) Population trajectories for two stochastic realizations of the co-evolution process with escape (in both cases, $q_c = q_{c,\infty} = 0.5$, $r = 0.1$, $d = 0.2$, $R = 2$, $M = 10^4$, $\mu = 5 \cdot 10^{-3}$, $\nu = 50$).

S7 Unified model of cancer-immune co-evolution

In this section we explore the level of diversity in behavior allowed by the co-evolutionary model with escape. We begin with a proof-of-principal for the relevance of an immune model by mapping differences in observed evasion rates to differential increases in cancer incidence. We then describe general features of the stochastic trajectories for reasonable parameter selection, and then apply the model to evolutionary cancer datasets.

S7.1 Evasion rates explain differential increases in early cancer incidence

We consider the relationship between early cancer incidence as an initial proof-of-principle of the relevance of immune surveillance parameterized in our model. In reality, it is known that immune system parameters vary temporally. We have shown previously that their variation is able fit well the AML age incidence curve [1]. Here, the immune turnover parameter parameterized by ν isolates the effects of T-cell turnover and detection efficiency rates from T-cell diversity. Since T-cell turnover is known to decline in early adulthood with preserved diversity [7], we hypothesize that differences in cancer evasion rates are reflected in differential increases in early age incidence. We assume that T-cell detection efficiency and turnover as well as the risk of tumor initiation are comparable.

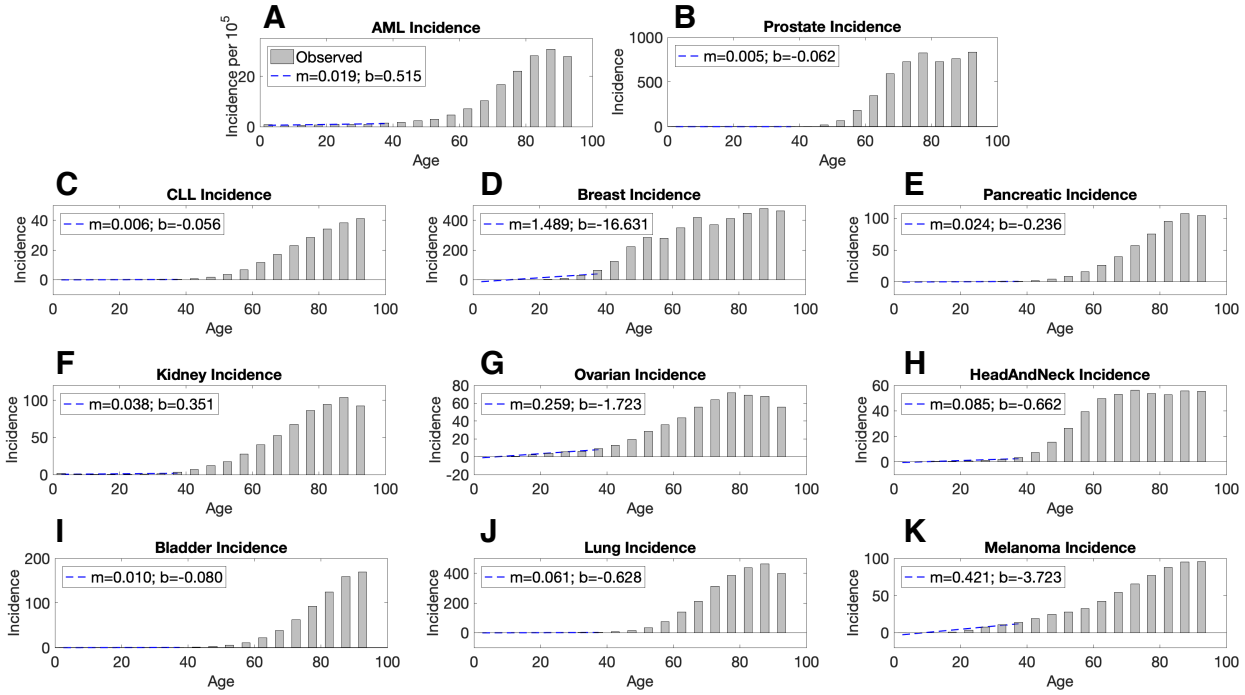

Figure S6: Cancer Incidence. Best-fit slope and intercept is obtained for early incidence data (from 0 to 37.5 years) for (A) AML; (B) Prostate; (C) CLL; (D) Breast; (E) Pancreatic; (F) Kidney; (G) Ovarian; (H) Head and Neck; (I) Bladder; (J) Lung; (K) Melanoma.

Toward this end, we restrict our analysis to the age interval between 0 and 40 years to omit the effects of significant declines in immune repertoire diversity. Our model would predict that subtype-specific differences in growth rates would also contribute to this difference. In the absence of reliable data on *in vivo* cancer-specific growth rates, we restrict our attention instead on evasion rates, using large patient repositories of per-cell mutation rates as a representative measure of this evasion [6]. We calculate lines of best fit to early cancer incidence data (obtained from cancerresearchuk.org)for a variety of cancer types (Fig. S6). Here,

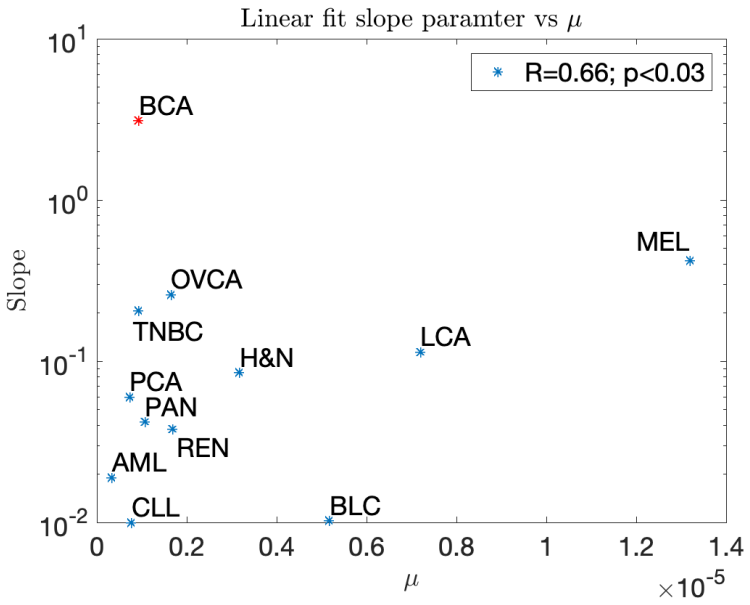

Figure S7: Cancer incidence and evasion rate. Rate of change in cancer early age incidence vs. evasion rate. For each age incidence curve, linear regression is performed for incidence in a similar manner as in Fig. S6, except that the regression input is restricted to values between minimal age at diagnosis and 40 years. The slope of the corresponding incidence curves are then plotted as a function of the per-cell mutation rate for each cancer type.

the positive slope parameters represent differential increases in each cancer type. Despite the dynamical complexities relating tumor progression and observed incidence, the slope of early cancer incidence correlates across many cancer types, both when applying linear regression at all ages between 0 and 40 (Fig. 4), and assuming a lower bound for age incidence at the minimum age at diagnosis (Fig. S7). In reality, the interplay between evasion (μ) growth (r), and detection (ν) rates are more complicated owing to cancer subtype-specific infiltration and immune presentation patterns, in addition to the clone-dependent values within a given tumor. and likely have a random component with each new clone and in turn define their success at producing progeny via λ in the subsequent recognition cycle. We remark that a more complete analysis would consider the distribution of values of μ, r, d that depend on particular driver clone. We find that breast cancer is one extreme element within the studied group, perhaps owing to increased reporting as a result of screening guidelines. Restricting our attention to TNBC tumors instead demonstrates statistically significant agreement (Pearson's correlation coefficient with hypothesis testing at significance level $\alpha = 0.05$).

S7.2 General model features

Fig. S8 illustrates an example trajectory, with colors indicating clones which arise from the same period. The first feature, cancer initiation, quantifies the likelihood that such a process would begin in the first place. We consider this to be either a rare or common event relative to underlying cancer incidence, and is independent of any model parameters. Clonotypic branching refers to the extent to which there is an increase in the number of distinct clones at each period and is completely determined by the branching parameter λ. Control of an evolving threat is the extent to which a threat stays in a state of non-escape and non-elimination, and is represented by clonal trunk length. Large clearance probabilities q_c result in longer clonal trunk lengths. The degree of branching λ inversely affects clonal trunk length since, all else equal, increases in λ augment the average number of clones available to escape during each period, thus shortening the number of periods prior to escape. Ultimate threat elimination is characterized by transformations T

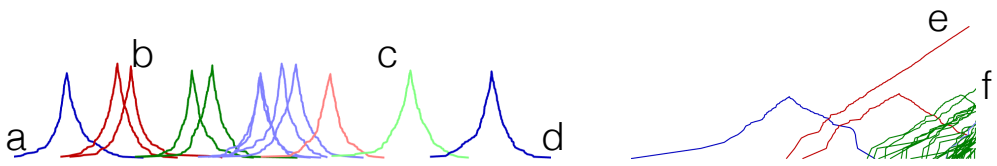

Figure S8: Features of the general co-evolutionary dynamical framework. (a) Cancer initiation, (b) degree of branching prior to escape, (c) level of control of the threat, (d) ultimate elimination, (e) ultimate escape, (f) branching due to escape.

and $\tilde{T}$, which are functions of branching and control. Escape likelihood is similarly characterized related to branching and control through $\tilde{T}$. The subsequent number of clones post-escape is approximated in Sec. S6.

The complete model affords significant flexibility in the allowable dynamical behavior. Below is a comprehensive characterization of all possibilities in the key determinants of this behavior and the resulting effect on predicted incidence and clonal evolution.

- I. (a) rare, (b) $\lambda \leq 1$, (c) q_c low : Incidence determined strictly by arrival (a). Escape arrives quickly after few cycles, and little to no branching observed.
- II. (a) rare, (b) $\lambda \leq 1$, (c) q_c high : Little to no branching. q_c large and $\lambda < 1$ implies that extinction dominates in the splitting probability of extinction vs escape, so that escape is rare. Together with (a) rare, this outcome is 'rare'[2].
- III. (a) rare, (b) $\lambda > 1$, (c) q_c low : Branching occurs early, shortening the clonal trunk of evolution. Multiple escape events are likely, leading to multiple sub-clones detectable post-escape.
- IV. (a) rare, (b) $\lambda > 1$, (c) q_c high : Possible extended evolution prior to absorbing state. Escape more likely due to $\lambda > 1$. Net branching shortens the average number of cycles prior to escape. unless $\lambda \sim 1$.
- V. (a) common, (b) $\lambda \leq 1$, (c) q_c low : Similar to I. but this time initiation occurs commonly, and in the majority of cases, leads to cancer escape and cancer incidence ('common'[2]).
- VI. (a) common, (b) $\lambda \leq 1$, (c) q_c high : Initiation common, but incidence is controlled by high immune functioning. Conditional on escape, there is a long clonal trunk when $\lambda \sim 1$.
- VII. (a) common, (b) $\lambda > 1$, (c) q_c low : Similar to III, but everyone commonly gets tumor initiation and subsequent disease, occurs more rapidly than V ('common'[2]).
- VIII. (a) common, (b) $\lambda > 1$, (c) q_c high : Initiation is common, but disease can be controlled by high clearance probability. Shorter clonal trunk expected due to rapid expansion of clone numbers and escape, assuming it occurs, happens earlier than in VI. supercritical λ also results in more detectable sub-clones post-escape than in V. Larger clonal trunks are observed when $\lambda \sim 1$.

Depictions of simulations involving combinations of branching parameter and control parameters are depicted in Fig. S9.

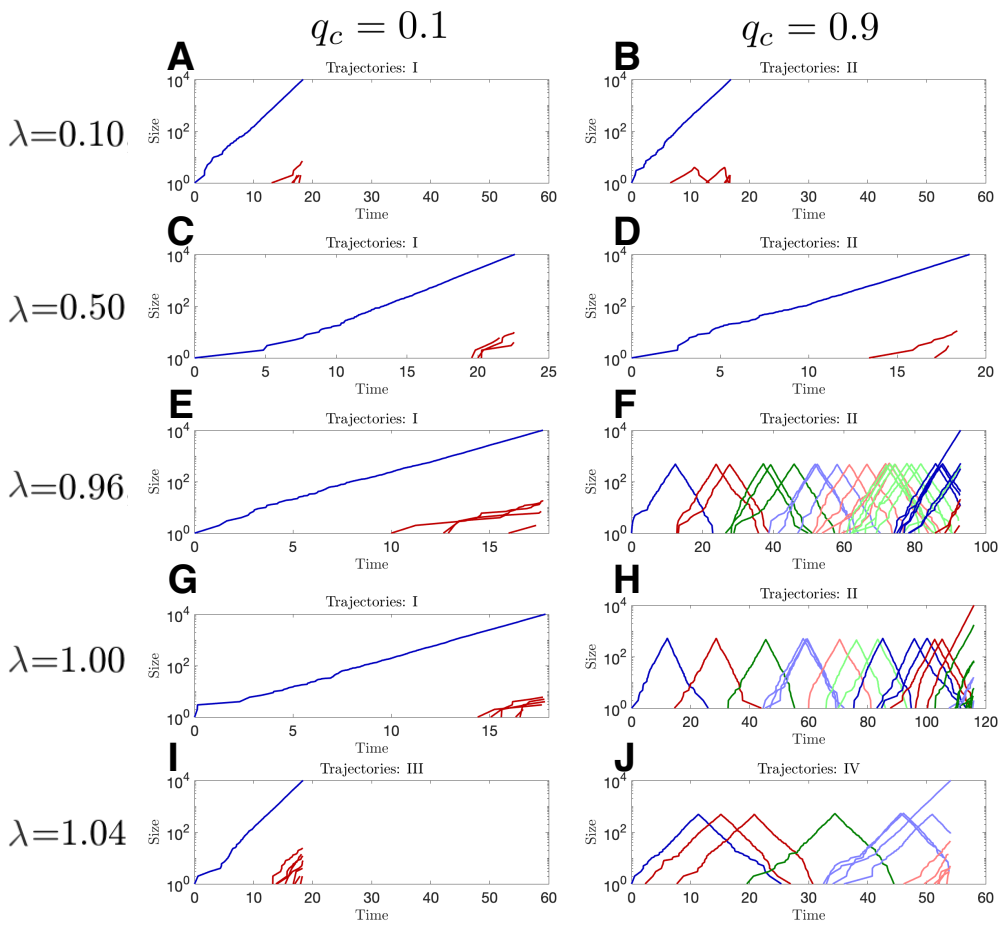

Figure S9: Typical stochastic trajectories. Representative trajectories for low branching, low control (A,C,E,G); low branching, high control (B,D,F,H); high branching, low control (I); and high branching, high control (J) (parameters chosen to generate reported branching parameters in adaptive recognitions simulations).

S7.3 Parameter selection

Immediately, II, V, VII appear to be unsuitable for realistic levels of cancer incidence. Of the remaining events where tumor initiation is rare, significant clonal evolution is not predicted in I or III, as evolution post-escape is purely sub-clonal. We keep in mind the remaining behaviors (IV, VI, VIII) in comparing model dynamics empirically observed cancer evolutionary data, and make an argument for VI and VIII (i.e. that real data is consistent with tumor initiation being a relatively common event, with progression and eventual escape the rare occurrence in a manner consistent with long periods of clonal evolution below detection size). In this section we derive a relevant parameter selection for actual tumor behavior, and restrict our attention to a reasonable behavior for tumor evolution.

S7.3.1 Detection size variability

In the deterministic case all populations are detected at size m_0. The variability in detection size, m, for a given clone in the adaptive case can be assessed by dividing the adaptive clone intensity in Eq. S72 by the per-cell intensity λ_0, giving

$$m \equiv \Lambda/\lambda_0, \tag{S103}$$

so that

$$\mathbb{E}[m] = \nu + m_0, \qquad \mathbb{V}\mathrm{ar}(m) = \nu. \tag{S104}$$

If detection is size-limited, as in [1], then $m_0 = R/r$ for R lower detectable total growth rate of a foreign threat. Without loss of generality, we take $d \equiv 1$ so that $r = r/d$, for $0 < r < 1$. If threats of most growth-rates are handled, then $\lambda = \lambda_0 m_0 \leq 1$ for a majority of growth rates r. Toward this end, we denote extreme choices of growth rate by $\varepsilon > 0$ be small so that $\lambda|_{r=\varepsilon,1-\varepsilon} = 1$. This implies that R may be written as $R = \varepsilon(1-\varepsilon)/\mu$. Additionally, the index of dispersion, $D(m)$, is

$$D(m) = \frac{\mathbb{V}\mathrm{ar}(m)}{\mathbb{E}[m]} = \frac{\nu}{\nu + m_0} = \frac{\mu\nu r}{\mu\nu r + \varepsilon(1-\varepsilon)}. \tag{S105}$$

The dispersion is plotted as a function of immune parameter ν and growth-rate r and compared alongside mean predicted detection sizes (Fig. S10). Our model predicts that the detection size of various clones is highly variable for larger growth rates, compared to that of small growth rates, which have smaller relative dispersion. The effect of impaired immunity is modeled by increasing ν, which also increases the level of dispersion.

This assumption on relevant sneak-through windows gives

$$m_0(r) = \varepsilon(1-\varepsilon)/\mu r, \qquad \tilde{\lambda} = \lambda + \lambda_0\nu = \frac{\mu}{1-r}\left[\frac{\varepsilon(1-\varepsilon)}{\mu r} + \nu\right]. \tag{S106}$$

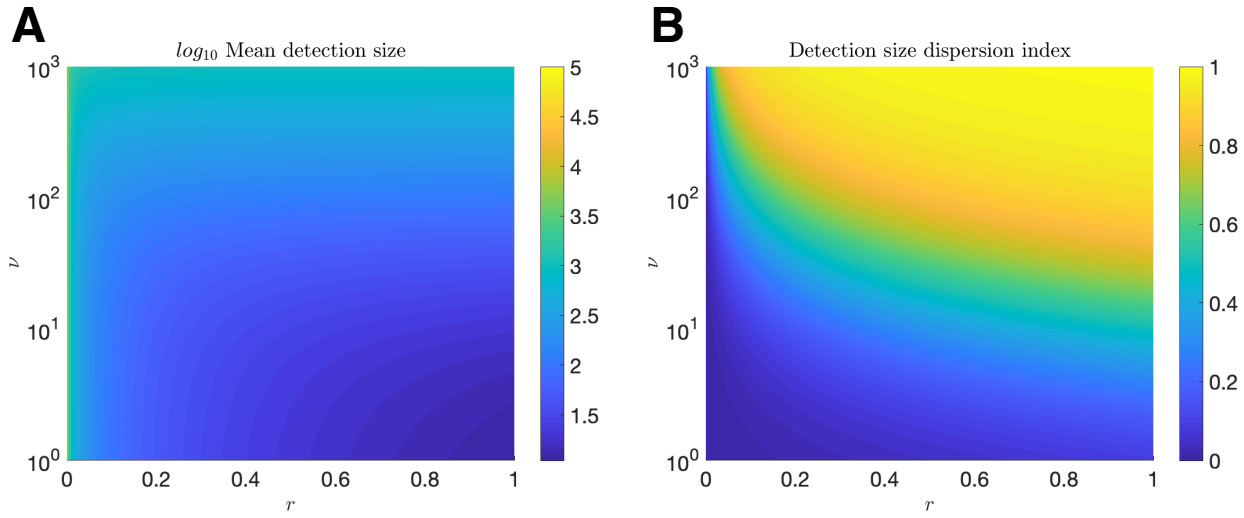

Figure S10: Detection size mean dispersion index. The detection size (A) mean, $\mathbb{E}[m]$, and (B) index of dispersion, $D(m)$, are plotted as a function of growth rate r and immune detection parameter ν ($\mu = 10^{-6}$, $\varepsilon = 10^{-5}$).

S7.3.2 Detection of large growth rate threats

Interesting threats are those which do not grow faster than the maximal immune killing rate d. In this case, we recall that

$$\lambda_0 = \mu/(1-r), \qquad m_0 = R/r, \qquad \lambda = \lambda_0 m_0 \tag{S107}$$

We make the assumption that the background detection size of an extremely fast-growth threat, independent of the adaptive parameter (i.e. via λ), is small (i.e. $m_0(r=1) \approx 1$). This assumption implies that $R = \varepsilon(1-\varepsilon)/\mu$ and imposes the following estimation of the sneak-through window ε:

$$m_0|_{r=1} \approx 1 = \frac{\varepsilon(1-\varepsilon)}{\mu}. \tag{S108}$$

Since $\varepsilon \ll 1$, this gives $\varepsilon \approx \mu$ for $\mu = 10^{-6}$. This subsequently implies that

$$m_0|_{r=\varepsilon} = \frac{1-\varepsilon}{\mu} \approx 1/\mu = 10^6, \qquad m_0|_{r=1-\varepsilon} \approx \varepsilon/\mu \approx 1. \tag{S109}$$

and

$$\tilde{\lambda}|_{r=\varepsilon} = 1 + \frac{\mu}{1-\varepsilon}\nu \approx 1 + \mu\nu = 1 + 10^{-6}\nu, \qquad \tilde{\lambda}|_{r=1-\varepsilon} = 1 + \mu\nu/\varepsilon \approx 1 + \nu. \tag{S110}$$

For an intermediate-growth threat ($r = 1/2$), we have

$$\lambda_0|_{r=1/2} = 2\mu = 2 * 10^{-6}, \tag{S111}$$

and

$$\tilde{\lambda}|_{r=1/2} = 4\mu + 2\mu\nu. \tag{S112}$$

S7.3.3 Common incidence, rare progression

More generally,

$$\tilde{\lambda} = \mu\left(\frac{1+\nu r}{r(1-r)}\right), \tag{S113}$$

with first order condition

$$\frac{\partial\tilde{\lambda}}{\partial r} = \left(\frac{\mu}{r^2(1-r)^2}\right)\left(\nu r^2 + 2r - 1\right) = 0, \tag{S114}$$

ultimately giving a minimal $r_* > 0$ of

$$r_* = \frac{\sqrt{1+\nu} - 1}{\nu}, \tag{S115}$$

with minima

$$\tilde{\lambda}(r_*) = \frac{\mu\nu^2}{\left(\sqrt{1+\nu} - 1\right)^2} \geq \mu\nu. \tag{S116}$$

Taken together, this implies that the host is most effective at minimizing the branching parameter at r_* depending inversely on immune compromise parameter ν, and that in the deterministic case with no compromise ($\nu = 0$), threats of intermediate growth rate $r_* = 1/2$ are maximally cleared. Moreover, branching for all values of $\varepsilon \leq r \leq 1-\varepsilon$ is bounded below (at $r = r_\star$) and above (at $r = 1-\varepsilon$) by

$$\mu\nu \leq \tilde{\lambda} \leq 1 + \nu. \tag{S117}$$

Finally, since

$$\frac{\partial\tilde{\lambda}}{\partial\nu} = \lambda_0 = \frac{\mu}{1-r}, \tag{S118}$$

we predict that the control of rapidly dividing threats is more sensitive to changes in adaptive immunity. Lower bounds on branching also provide the following condition on immune compromise after which threats of all growth rates are predicted to branch as $\nu > \mu^{-1}$. This predicts that threats with larger mutational rates have an easier time overcoming adaptive immunity as it becomes compromised, regardless of growth rate.

Together, we conclude that under normal adaptive immunity, $\lambda \leq 1$ appears to be reasonable should threats of a large variety of growth rates be containable, in support of hypotheses I, II, V, VI above. Intersecting this with earlier remarks give us our working model of cancer evolution via scenario VI. From this, we predict that the frequency of tumor initiation is significantly more common relative to ultimate incidence, which is due to the low probability of escape and sub-critical branching that leads to ultimate elimination in most cases. In the next section, we rely on available data to quantify its extent.

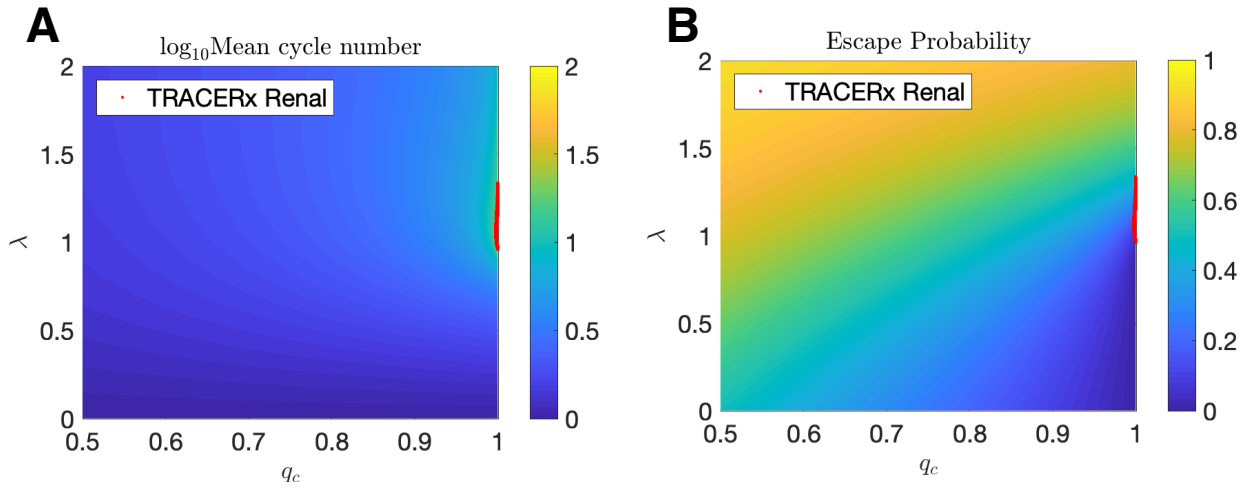

Figure S11: Mean recognition cycles and Escape probabilities assuming rare initiation. (A) $\log_{10}$ mean number of recognition cycles and (B) cancer escape probabilities as a function of q_c and λ for deterministic recognition evaluated using tie probabilities in Eq. S56.

S7.4 Renal cancer evolution predicts common cancer initiation with rare progression to disease

Recent innovation enabling the tracking of evolutionary trajectories in large patient datasets has provided new opportunities to study early cancer initiation and progression that ultimately leads to disease. The primary advantage of such studies related to our analysis is in their retrospective estimation of cancer initiation and progression. In the first case, early evolutionary data for clear cell renal cell cancer (ccRCC) is analyzed from the TRACERx renal consortium [9]. The authors of this study find, perhaps surprisingly, that the evolution of renal cancer is characterized by a prolonged state of little to no net growth (5-20 years) sustained by populations below detection level (estimated to be on the order of hundreds of cells), eventually followed by escape and ultimate diagnosis. We argue that this prolonged state can be explained by effective co-evolution proposed above, and that the length of time in such a state has implications for the relative rate of tumor initiation.

In the aforementioned study, sequencing was performed at an average depth of 64X on 95 biopsies from 33 patients and revealed an average of 1,193 in-frame deletions and 7,680 somatic substitutions per patient. We assume that these changes correlate with any possible immune evasion, and that a small subset (0.1% to 1%) actually represent immunologically-relevant evasion events, for which we expect somewhere between 8 to 80 events relevant to co-evolution. We next attempt to approximate this value from below using experimentally estimated times to most recent common ancestor (MRCA), t_m and ultimate detection, t_M. We assume that the population of the escaping clone at detection is $X(t_M) = M \sim 10^9$. Similarly, $X(t_m) = m_0 \sim 10^2$ based on TRACERx estimates. If no co-evolution occurs and the population undergoes exponential expansion then the timing of escape depends linearly on the logarithmic population, so that $9t_m/2 = t_M$, and the intervening time between MRCA and escape, $\Delta t = t_M - t_m = 7t_m/2$. If instead n cycles occur prior to escape and we assume that progeny occur approximately at the peak of population size, then the intervening time is instead $\Delta t = t_M - nt_m$. In both cases, escape takes the same amount of time so that $\Delta t = 7t_m/2$ giving

$$7t_m/2 = t_M - nt_m. \tag{S119}$$

Since t_M and nt_m are measured, we can estimate the number of recognition cycles, n, by

$$n = \frac{7nt_m}{2(t_M - nt_m)}. \tag{S120}$$

Using the 31 available times in the TRACERx renal consortium, we estimate an average of $n = 26.6$ recognition cycles in renal cancer. This together with the mutational signature suggests 0.3% of observed mutational events correspond with relevant immune evasion. We use a modified version of Eq. S38 conditioned on ultimate escape (E_∞), given by

$$\mathbb{P}(\tilde{E}_n \mid E_\infty) = \left(T^{n-1}1 - T^n 1\right)/(1 - p^*), \tag{S121}$$

to calculate cycle number N conditional mean and variance,

$$\mathbb{E}\left[N \mid E_\infty\right] = \sum_{n=0}^{\infty} n\mathbb{P}(\tilde{E}_n \mid E_\infty) \tag{S122}$$

$$\mathbb{V}\mathrm{ar}\left(N \mid E_\infty\right) = \sum_{n=0}^{\infty} n^2\mathbb{P}(\tilde{E}_n \mid E_\infty) - \left(\sum_{n=0}^{\infty} n\mathbb{P}(\tilde{E}_n \mid E_\infty)\right)^2. \tag{S123}$$

From this, we identify regions of parameter space where the observed number of recognition cycles occurs (Fig. S11). It is of no surprise that the mean number of recognition cycles becomes large when the branching parameter λ is concentrated at criticality (Fig. S11A). We note that super-critical branching is expected not only to decrease mean recognition cycle number, but also progression period since control of a branching threat on average requires the occurrence of more evasion events in the same time period as a non-branching

threat.

With this in mind, we focus our analysis to $0 < q_c, \lambda < 1$. Relevant average recognition cycle number is generally predicted for high clearance probability ($q_c \geq 0.9$) whenever $\lambda > 0.9$. We note that cancer incidence requires tumor escape following an initiation event (Fig. S8). While initiation necessarily cannot occur at a frequency less than cancer incidence, its rate may exceed actual incidence. In one extreme case, initiation might be a rare event so that the majority of incidence is explained by rare initiation that invariably leads to escape and cancer diagnosis. In this case, referred to as 'rare initiation, common progression,' co-evolution would have a weak or non-existent effect on overall incidence as escape probabilities would approach one so that progression nearly always leads to disease. On the other hand, under 'common initiation, rare progression,' originating cancer risks arrive at a significantly higher frequency than measured incidence. In this case, the model predicts co-evolution to be a substantial contributor to observed incidence as low escape probabilities filters many frequent initiation events.

Mean recognition cycles are plotted as a function of $1 - q_c$ and $1 - \lambda$ with estimated mean cycle number highlighted (Fig. 5A). Relevant clearance probabilities are predicted to be high, implying that the model predicts effective interrogation of and recognition against many threats. From this, the parameter selection that overlaps with maximal observed escape probability suggests that renal cancer initiation is 18 times as likely as observed incidence (Fig. 5C), in support of the 'common initiation, rare progression' hypothesis. The above theory provides a method of assessing the predicted balance between initiation and co-evolutionary escape as contributors to overall incidence, given cancer incidence data and estimates of the progression period. In summary, cancers with large progression periods exist close to criticality ($\lambda \leq 1$) and have large clearance probabilities, which results in concomitant increases in recognition period and cycle number. Based on the above theory, this case is predicted to have random and frequent arrivals of initiating clones relative to observed incidence, with co-evolution providing an important contribution to incidence by filtering many of these cases with a low escape probability. We remark that estimates of mean cycle number are most sensitive to the assumed minimal detection window at which threats are eliminated. We assumed $m_0 = 100$ in order to match TRACERx estimates. Repeating the analysis for $m_0 = 1,000$ generates a mean recognition cycle number of $n = 15.2$. In conclusion, the extent of common initiation as a multiple of observed incidence is predicted to vary directly with progression period (i.e. mean number of recognition cycles). Examples of clonal and total population trajectories for recognition followed by ultimate control or escape is given in Fig. 5B,D under deterministic recognition assuming initiation is 18 times as frequent as incidence.

We partition the data utilized in Fig. 5A.C into two groups: Evolution dominated by linear evolution or branched evolution. TRACERx samples were assigned to the former group in absence of substantial branched evolution prior to escape (determined by having the difference in arrival time of MRCA to escape less than 10 years), giving 13 total samples dominated by linear evolution and 19 dominated by branching. The previous analysis was applied similarly to both of these groups in order to determine the expected mean cycle number (Fig. S12A) and frequency of escape relative to initiation (Fig. S12B). We find that branching evolution and early, likely escape are concomitant, while sustained linear evolution indicates sustained co-evolution with common incidence, rare progression. Branching evolution was found to have 5 ± 2 ($\mu \pm \sigma$) recognition cycles, with initiation predicted to occur five times as frequently as observed incidence. In contrast, linear evolution was characterized by 57 ± 35 recognition cycles, with initiation 41 times as likely as observed incidence. In comparing the disease severity of each of these groups based on histological grade, we find non-statistically significant increase in disease severity corresponding with evolution dominated by branched evolution. This approach demonstrates the model's ability to assess cancer evolutionary paths with respect to disease severity and, ultimately, treatment prognosis. Future analysis of large-sample studies would help to better characterize this relationship.

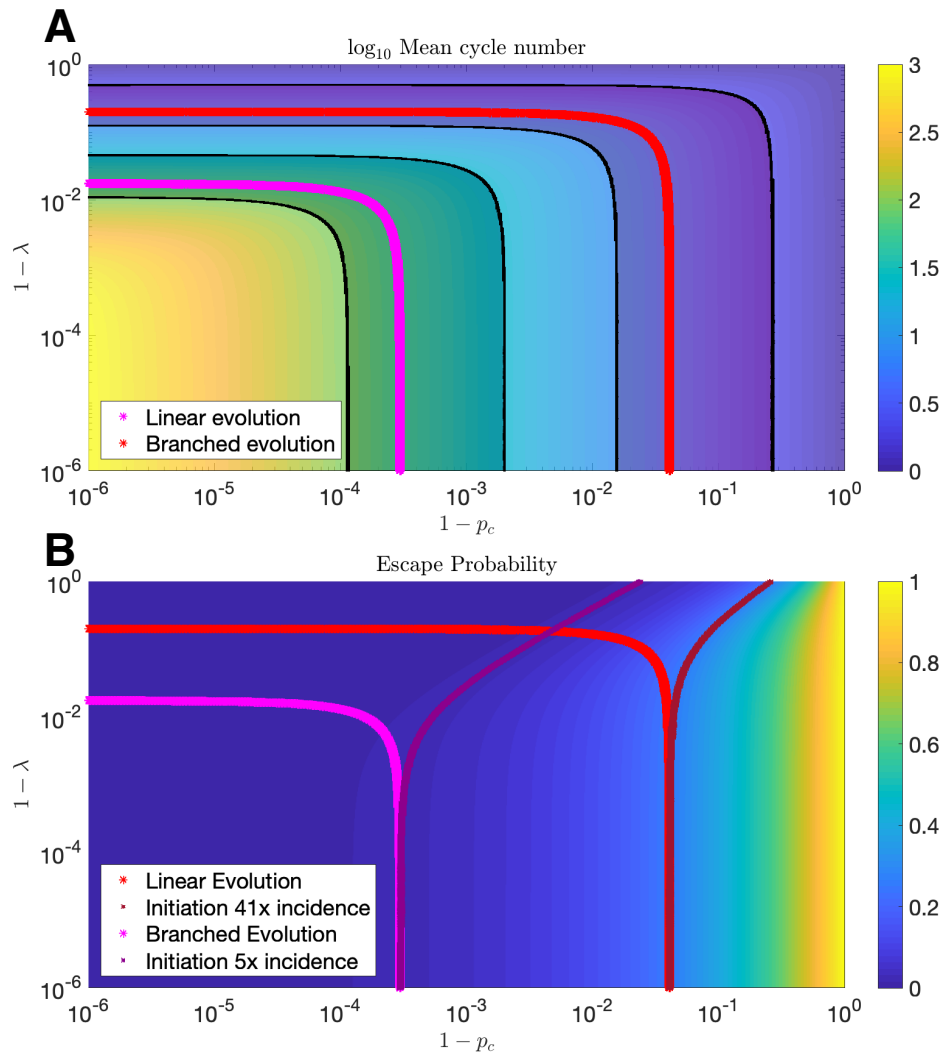

Figure S12: Cycle number and cancer frequency for linear vs branched evolution. (A) Estimated mean cycle number ± 1 standard deviation (shaded region) is plotted for samples with predominant linear and branched evolution as a function of clearance probability and branching parameter; (B) Maximal escape probabilities are calculated assuming the estimated mean cycle number.

S7.5 Smoking status correlated with predicted immune surveillance impairment in early-stage non-small cell lung cancer

In a similar way as above, the tracking of landmark evolutionary events was performed for non-small cell lung cancer (NSCLC) [3]. Whole exome sequencing was performed on 327 tumor regions from 100 patients with NSCLC and no prior treatment. The authors found significant correlation between the number of early mutations and tobacco exposure, and identified mutations induced by tobacco, which consequently had direct influence on the clonal trunk length (i.e. the number of mutations in the MRCA). Last of all, the authors find a long period of what appears to be tumor latency in the evolution of lung adenocarcinoma before clinical presentation, in a similar manner as in ccRCCC.

This data, which provides subtype-specific mean and variance estimates of clonal trunk length, allows us to use our statistical framework to predict the differences in immune relevant model parameters that

Table S1: TRACERx Estimated NSCLC Mutation Burden

Subcategory	Clonal mutations, Ω	
	Mean, μ_Ω	Variance, σ^2_Ω
All LCA ($n = 100$)	489	$2.26 \cdot 10^5$
Smoker ($n = 48$)	526	$2.23 \cdot 10^5$
Nonsmoker ($n = 14$)	255	$1.91 \cdot 10^5$
Adenocarcinoma ($n = 61$)	447	$2.86 \cdot 10^5$
Squamous-cell carcinoma ($n = 32$)	573	$1.40 \cdot 10^5$

distinguish each disease. As in the ccRCC case, we assume that a small fraction, $\alpha \ll 1$, of the total mutational signature is immunologically relevant. If Ω is the total number of observed mutations with $\mu_\Omega = \mathbb{E}[\Omega]$ and $\sigma^2_\Omega = \mathbb{V}\mathrm{ar}(\Omega)$, then there is a quadratic relationship between the mean and variance fraction of relevant mutations, $\alpha\Omega$ parameterized by α, namely,

$$\mathbb{E}[\alpha\Omega] = \mu_\Omega \alpha \tag{S124}$$

and

$$\mathbb{V}\mathrm{ar}(\alpha\Omega) = \sigma^2_\Omega \alpha^2. \tag{S125}$$

Plots of the mean-variance frontier are given for all sample subtypes (Fig. 6). For normal, deterministic recognition, there is an upper limit on the allowable variance-to-mean ratio observed across all possible parameter choices. The allowable region in the adaptive case overlaps nearly entirely with that of the deterministic case, but also permits lower values of variance relative to the mean. We refer to the non-overlap as the region of immune impairment, since, all else equal, these values are only possible with the addition of a strictly positive adaptive parameter, thus increasing recognition above the lower allowable detection limit m_0. It is in general difficult to observe increases in the variance-to-mean ratio above those observed in the deterministic case. We found that adding an assumption of temporal immune enhancement over time, where the clearance probability may increase toward an upper limit ($q_{c,\infty} = 0.90$ in our case) according to

$$q_{c,n+1} = \max\{q_{c,\infty}, q_{c,n} + (p_{c,n} - q_{c,\infty}/25)\}, \tag{S126}$$

generates behavior that overlaps with the non-nonsmoker and lung adenocarcinoma cases. The non-overlap region with high relative variance is likely due to trajectories with initially low clearance probabilites that increase to the upper limit over time. Our results suggest that in addition to the larger mutational burden of smokers' LCA, non-smokers benefit from being able to control initiating cancer threats with an immune system which may augment its anti-tumor ability slowly over time. This is in contrast to smokers and squamous cell carcinoma, both having mean-variance frontiers more consistent with systems having appreciable compromises in their immune ability through reduced detection rates resulting from larger minimal detection sizes.

References

[1] Jason T George and Herbert Levine. Stochastic modeling of tumor progression and immune evasion. *Journal of theoretical biology*, 458:148–155, 2018.

[2] Geoffrey Grimmett and David Stirzaker. *Probability and random processes*. Oxford university press, 2001.

[3] Mariam Jamal-Hanjani, Gareth A Wilson, Nicholas McGranahan, Nicolai J Birkbak, Thomas BK Watkins, Selvaraju Veeriah, Seema Shafi, Diana H Johnson, Richard Mitter, Rachel Rosenthal, et al. Tracking the evolution of non–small-cell lung cancer. *New England Journal of Medicine*, 376(22):2109–2121, 2017.

[4] Samuel Karlin. *A first course in stochastic processes*. Academic press, 2014.

[5] Catherine M Koebel, William Vermi, Jeremy B Swann, Nadeen Zerafa, Scott J Rodig, Lloyd J Old, Mark J Smyth, and Robert D Schreiber. Adaptive immunity maintains occult cancer in an equilibrium state. *Nature*, 450(7171):903, 2007.

[6] Michael S Lawrence, Petar Stojanov, Paz Polak, Gregory V Kryukov, Kristian Cibulskis, Andrey Sivachenko, Scott L Carter, Chip Stewart, Craig H Mermel, Steven A Roberts, et al. Mutational heterogeneity in cancer and the search for new cancer-associated genes. *Nature*, 499(7457):214, 2013.

[7] Keith Naylor, Guangjin Li, Abbe N Vallejo, Won-Woo Lee, Kerstin Koetz, Ewa Bryl, Jacek Witkowski, James Fulbright, Cornelia M Weyand, and Jörg J Goronzy. The influence of age on t cell generation and tcr diversity. *The Journal of Immunology*, 174(11):7446–7452, 2005.

[8] H Schreiber, TH Wu, J Nachman, and WM Kast. Immunodominance and tumor escape. In *Seminars in cancer biology*, volume 12, pages 25–31. Elsevier, 2002.

[9] Samra Turajlic, Hang Xu, Kevin Litchfield, Andrew Rowan, Tim Chambers, Jose I Lopez, David Nicol, Tim O'Brien, James Larkin, Stuart Horswell, et al. Tracking cancer evolution reveals constrained routes to metastases: Tracerx renal. *Cell*, 173(3):581–594, 2018.